UHASSELT
KNOWLEDGE IN ACTION

Maastricht University

Faculty of Medicine and Life Sciences
School for Life Sciences
Master of Biomedical Sciences

Master's thesis

Characterization of in vitro salivary gland models to investigate the radioprotective effect of amifostine after prostate cancer radiation therapy

Rosanne Breugelmans

Thesis presented in fulfillment of the requirements for the degree of Master of Biomedical Sciences, specialization Environmental Health Sciences

SUPERVISOR :
Prof. dr. Michelle PLUSQUIN

SUPERVISOR :
dr. Koen VERMEULEN

MENTOR :
mevr. Nathalie HEYNICKX

2021
2022

Transnational University Limburg is a unique collaboration of two universities in two countries: the University of Hasselt and Maastricht University.

UHASSELT
KNOWLEDGE IN ACTION

www.uhasselt.be
Universiteit Hasselt
Campus Hasselt:
Martelarenlaan 42 | 3500 Hasselt
Campus Diepenbeek:
Agoralaan Gebouw D | 3590 Diepenbeek

UHASSELT
KNOWLEDGE IN ACTION

Maastricht University

Faculty of Medicine and Life Sciences
School for Life Sciences
Master of Biomedical Sciences

Master's thesis

Characterization of in vitro salivary gland models to investigate the radioprotective effect of amifostine after prostate cancer radiation therapy

Rosanne Breugelmans

Thesis presented in fulfillment of the requirements for the degree of Master of Biomedical Sciences, specialization Environmental Health Sciences

SUPERVISOR :
Prof. dr. Michelle PLUSQUIN

SUPERVISOR :
dr. Koen VERMEULEN

MENTOR :
mevr. Nathalie HEYNICKX

Characterization of *in vitro* salivary gland models to investigate the radioprotective effect of amifostine after prostate cancer radiation therapy*

Rosanne Breugelmans[1], Nathalie Heynickx[2,3], Michelle Plusquin[1], Koen Vermeulen[4]

[1]Centre for Environmental Sciences, Hasselt University, Diepenbeek, Belgium

[2]Institute for Environment, Health and Safety, Radiobiology Unit, Belgian Nuclear Research Centre (SCK CEN), Mol, Belgium

[3]Department of Molecular Biotechnology, Ghent University, Ghent, Belgium

[4]NURA, Belgian Nuclear Research Centre (SCK CEN), Mol, Belgium

**Running title: Salivary gland models to investigate amifostine*

To whom correspondence should be addressed: Koen Vermeulen, Tel: +32 14 33 88 12; Email: koen.vermeulen@sckcen.be

Keywords: PSMA-targeted radionuclide therapy, amifostine, salivary gland damage, prostate cancer, external beam radiotherapy (list at least 5 keywords)

Abstract

Salivary gland toxicity remains an important side-effect during [^{177}Lu]Lu-PSMA-617 therapy targeting disseminated prostate cancer. A 3D culture is expected to be more relevant to study functional damage due to the formation of acinar structures and the increased expression of AQP-5 and NKCC1. Radioprotectors, such as amifostine, could protect the salivary glands during treatment. Amifostine has to be converted to its active metabolite by alkaline phosphatase expressed in healthy cells and downregulated in cancer cells. A-253 3D salivary gland cell culture was optimized using different concentrations of Matrigel®. Optimization of NKCC1 and AQP-5 protein detection by western blot was performed using different blocking buffers and different concentrations of primary antibodies on A-549 and HK-2 cells. Alkaline phosphatase activity was measured in PC3-Flu, PC3-PIP, and A-253 cells with the Alkaline Phosphatase Diethanolamine Activity Kit. Cytotoxicity of amifostine was investigated with sulforhodamine B staining assay. The radioprotective effect of amifostine after exposure to 0, 2 or 5 Gray (X-rays) was investigated with an MTS assay. A successful 3D culture was formed. Nonspecific antibody binding was detected for the AQP-5 primary antibody, while a specific band for NKCC1 could be observed on A-549 cells and not in HK-2 cells. A-253 cells showed higher alkaline phosphatase activity compared to PC3-PIP and PC3-Flu cells (p-value<0.0001). The highest concentrations of amifostine indicated cytotoxic effects. The effects of amifostine during EBRT were inconclusive. Additional experiments are warranted to optimize AQP-5 expression and

determine cytotoxic and protective effects of amifostine during EBRT.

INTRODUCTION

Prostate cancer is, after lung cancer, the most common type of cancer in men worldwide (1). In 2020, 1.4 million new cases were diagnosed worldwide (2-6). Treatment options depend on the disease stage at diagnosis (7). While for early disease stage active surveillance and monitoring of prostate-specific antigen (PSA) levels often suffice, advanced disease requires more drastic treatment options such as surgery, external beam radiation therapy (EBRT) and hormonal therapy (mainly androgen deprivation therapy) (4, 8-10).

When prostate cancer is diagnosed in an early, localized stadium, the 5-year survival rate is nearly 100% (11). However, for patients with hormone-sensitive metastatic disease, survival rates drops to approximately 30 % (3, 11). In nearly 25% of the patients receiving hormonal therapy, the prostate cancer cells will become insensitive to androgen deprivation within 18 months, and metastatic castration-resistant disease (mCRPC) will occur (3, 12, 13). To date, no effective treatment is available for patients in this disease stage, as illustrated by a subsequent significant drop to a 5-year survival rate of approximately 15% and median survival around 18 months (3, 8, 14). Because of this, there is a high need to develop new and more effective treatment methods.

Prostate-specific membrane antigen (PSMA), a type II membrane glycoprotein, is an interesting target for prostate cancer treatment (15). The potential of PSMA as a target for the treatment of prostate cancer can be explained by the overexpression of PSMA on the cell membrane of prostate cancer cells, which is approximately 1000x higher compared to normal prostate cells. Also, this expression is further increased in the mCRPC disease stage (3, 16, 17). PSMA is a zinc-dependent metallopeptidase and is thought to have a role in multiple cellular activities. It

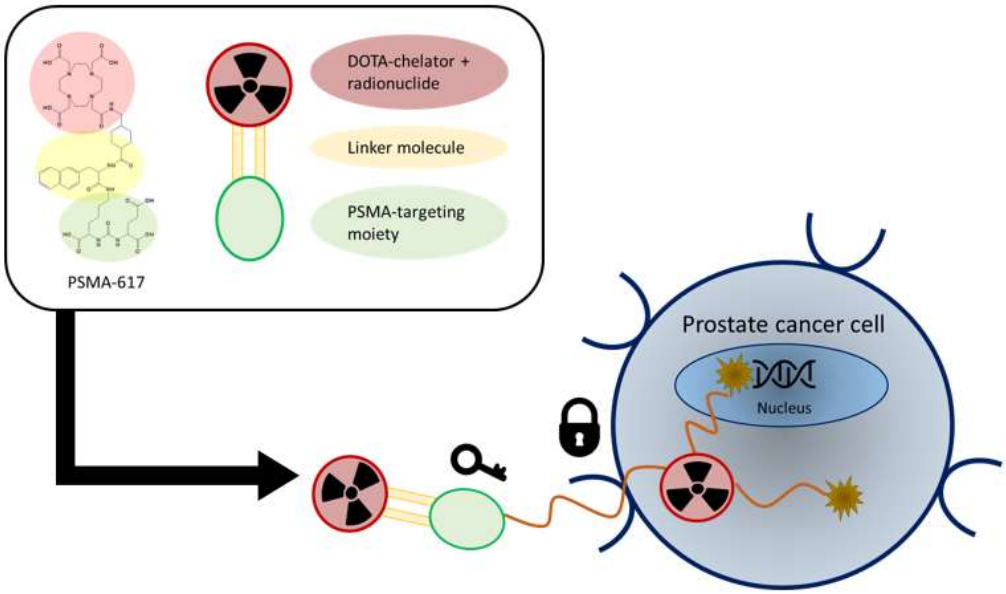

Figure 1: Visualization of the principle PSMA-targeted therapy. PSMA (visualized by the blue circles) is overexpressed on the cell membrane of prostate cancer cells. A PSMA-targeting molecule is linked to a radionuclide, emitting ionizing radiation (damaging pathway highlighted in yellow) to target and kill prostate cancer cells. PSMA = prostate-specific membrane antigen.

catalyzes the hydrolysis of N-acetylaspartylglutamate to N-acetylaspartate and glutamate (18, 19). However, the function of these enzymatic activities on prostate tissue remains largely unknown (20, 21). On top of its overexpression on prostate cancer tissue, the large extracellular domain of PSMA makes it an accessible and interesting target for targeted therapy (22, 23). When a ligand binds to PSMA, the ligand-receptor complex is internalized via receptor-mediated endocytosis, enabling interaction with the cell machinery (16, 20, 24-26). PSMA-targeted therapy (PSMA-TRT) combines the targeting capacity of a PSMA-targeted molecule with a toxic radionuclide to deliver ionizing radiation to the prostate cancer cells (figure 1) (27, 28). Importantly, PSMA expression is not limited to prostate cancer cells, as PSMA expression has also been reported in several healthy organs such as the kidneys, salivary glands and duodenum (3, 17). However, this expression is much lower in comparison to the prostate cancer cells but remains important to take into account regarding potential side effects (3, 17).

TRT makes use of radionuclides. Radioactive decay originates from an unstable nucleus. To compensate for this instability, energy will be released under the form of electromagnetic or particle radiation, which is routinely used in nuclear medicine (29, 30). Different types of radioactive decay exist. In α–decay, a helium core (consisting of two protons and two neutrons) is emitted, which has a high linear energy transfer (LET, the amount of energy lost by an ionizing particle per unit length of track) of 50–230 keV/μm, and a short tissue range (50-100 μm), causing a lot of damage to a small area (figure 2) (31-34). An example of an α-emitter is actinium-225, which is proven to be very effective in killing cancer cells by making double-stranded DNA breaks (33, 35-37).

Another form of particle decay is the emission of β-particles, subdivided into electron (β^-) and positron (β^+) emissions (38, 39). Based on the core structure of the radionuclide (excess of neutrons or protons), a β^--particle (electron) or a β^+-particle (positron, a positively charged electron) will be emitted. They are smaller compared to α-particles, have a LET of 0.1–1.0 keV/μm and a tissue range of 2-10 mm (figure 2) (31, 38-41). β^+-and β^-decay is respectively used in positron emission tomography (a diagnostic non-invasive imaging technique) and targeted radionuclide therapy. An example of a β^--emitter is lutetium-177, which has been successfully coupled to a carrier molecule targeting PSMA.

This compound, [^{177}Lu]Lu-PSMA-617, has already been demonstrated to have a significant effect on PSA levels in the clinic (25, 42, 43). VISION, a phase III clinical trial, investigated the efficacy and safety of [^{177}Lu]Lu-PSMA-617 in patients with mCRPC disease. Consequently, in March 2022, [^{177}Lu]Lu-PSMA-617 was approved as a standard therapy for prostate cancer by the Food and Drug Administration (FDA) (43-46).

The third mode of radioactive decay concerns the emission of γ-rays, which exist as high energy electromagnetic radiation. γ-rays originate from the unstable nucleus, and X-rays are generated as a secondary effect of nuclear decay (electron capture or slowing down of an electron). This type of radiation can be used for diagnostic imaging (47-49). Additionally, Auger-Meitner electrons, also originating as a secondary effect of nuclear decay, have a very high LET (4 to 26 keV/μm) and an even shorter tissue range than α-particles (<100 nm)(figure 2)(50-52). An example of a radionuclide that emits Auger electrons is iodine-125. To be effective, the Auger emitter has to be in close proximity to the cell nucleus or other organelles (such as the mitochondria) (50, 53-57).

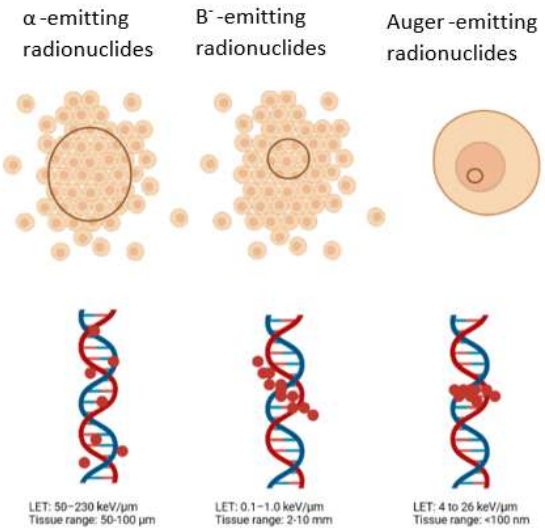

Figure 2: Overview of the different types of ionizing radiation used in TRNT. β^--particles will have the highest traveling distance, which can span several cells, over which the energy is divided. Thus are best used to target bigger tumors. α-particles are much bigger and hence will only travel a short distance, but the energy deposited over the traveled distance will be many times higher. Radionuclides emitting α-particles are best used targeting smaller tumors or metastatic lesions. The energy of Auger electrons will be emitted in a very small area and will be highly potent when this occurs in the proximity of the cell nucleus.

Even though PSMA expression is much higher on the cell membrane of prostate cancer cells, there still is a significant uptake of PSMA-targeted molecules in other, healthy tissue (3, 58) (59). These organs include the salivary glands, intestines and kidneys. Exposure of these organs to ionizing radiation can cause unwanted damage and side effects (3, 17, 60). Commonly reported side effects after [^{177}Lu]Lu-PSMA-617 therapy are fatigue, headache, dry mouth (xerostomia) and vomiting (3, 60, 61). The biggest concerns are raised of the toxicity to the kidneys and the salivary glands (3, 62, 63). However, until today, there is no clear evidence of kidney toxicity (3, 64, 65). On the other hand, salivary gland toxicity, and more specifically xerostomia (=also known as dry mouth syndrome), is a commonly reported side effect (3, 62, 63). Dysfunction of the salivary glands can cause various problems due to their importance in food digestion, protection of the oral mucosa and moistening of the palate for articulation (66). [^{177}Lu]Lu-PSMA-617 can affect the volume, consistency and pH of secreted saliva (67).

The uptake mechanisms of PSMA-targeted molecules by the salivary glands remain poorly understood, even though the uptake was already proven via positron emission tomography (figure 3B)(68, 69). Only a limited number of published studies are available, potentially due to the lack of available proper preclinical models of the salivary glands as a result of the complexity of the human salivary glands (Figure 3A) (3, 70-74). It was already shown that the acinar cells suffer from damage after exposure to external radiation ten days after exposure (75).

In addition, the use of animal models is limited. Some animal studies were already performed to reveal the mechanisms behind salivary gland damage in rodents (3, 76-79). Involvement of apoptosis, induced by p53, was shown (76). The translation of these results to humans remains difficult due to differences in PSMA-expression profiles between humans and the most commonly used laboratory animals (e.g. mice and rats (3, 80, 81). Pigs have the most similar PSMA-expression profile compared to humans, but they are difficult to use as a laboratory animals due to practical reasons (81). So the development of a reliable *in vitro* model can be a valuable asset due to the difficulty of translation from *in vivo* models (3).

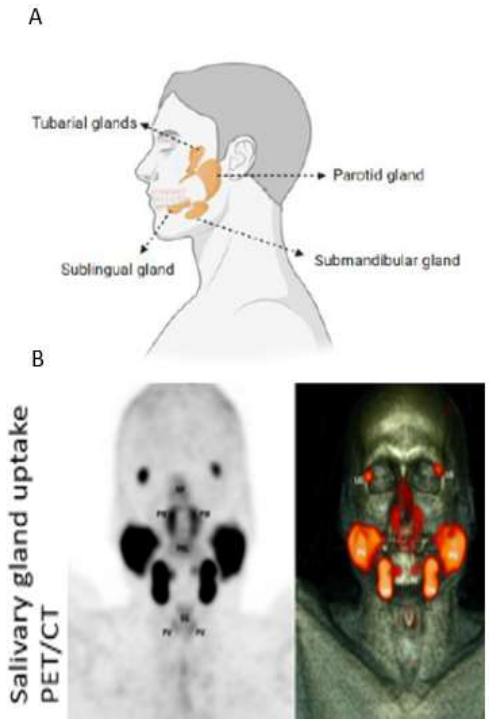

Figure 3: The human salivary glands (3) (82). (A) Anatomical visualization and localization of the major human salivary glands. (B) PSMA-targeted molecules are taken up significantly by the salivary glands, even though the PSMA expression is much lower in comparison to the prostate cancer cells. This can cause side effects like xerostomia or hypofunction of the salivary glands.

External beam radiotherapy (EBRT), currently used to treat multiple cancers, including breast-, lung-, head- and neck cancer, was shown to have a damaging effect on the salivary glands due to their location in the irradiation area (82-88). This effect is characterized by a loss in cellular function prior to a loss in the number of cells (3, 67, 89). Also, p53 expression was shown to be involved in salivary gland damage after exposure to EBRT (3, 76). The knowledge gained from literature, combined with the knowledge of these studies, can be used as a starting point to study the effect of PSMA-TRT on the salivary glands. Due to the loss of function prior to the loss of cells, it might be that changed protein expression levels are involved in the toxicity mechanisms (3, 67, 89). Because of this, it was chosen to focus on the expression profiles of NKCC1 and AQP-5 due to their importance in the secretion of saliva (90-92).

Due to the discomfort caused by xerostomia, research is being performed to reduce uptake in healthy tissue or to reduce salivary gland toxicity after PSMA-TRT by using radioprotectors (3). An Example is the prodrug amifostine (WR-2721), transformed *in vivo* to the active thiol metabolite (WR-1065), which can protect the cell by stabilizing DNA and upregulating p53 (figure 4) (93, 94). Importantly, alkaline phosphatase is needed for the conversion to its active thiol metabolite, which is downregulated in cancer

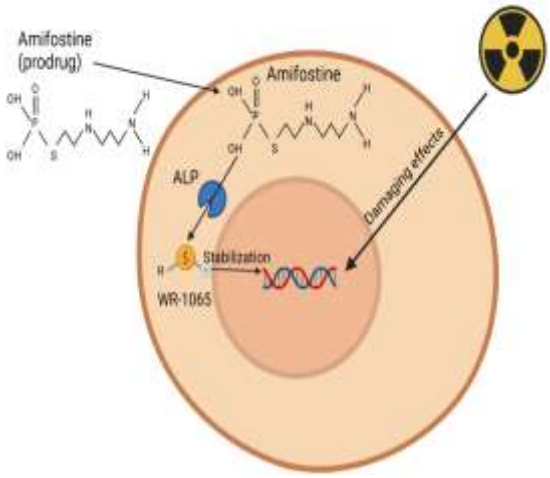

Figure 4: Radioprotective effects of amifostine. External beam radiotherapy will have damaging effects on the cells. This can be prevented by radioprotectors like amifostine, which is converted to its active thiol metabolite (WR-1065) by alkaline phosphatase. WR-1065 has protective effects on the cell by stabilizing the DNA. Alkaline phosphatase is downregulated in cancer cells and will convert amifostine to its active thiol metabolite only sparsely. ALP = alkaline phosphatase

cells (93, 94). Because of this, it can be expected that treatment with the prodrug amifostine will have protective effects on the healthy salivary glands, while the protective effect on the cancer cells will be minor (3, 93, 95). The cytoprotective effect of amifostine involves free radical scavenging, repair acceleration and DNA protection (96). Amifostine is approved by the FDA as a radioprotector during EBRT because it was already shown to reduce xerostomia after EBRT (66, 67, 97-99). Unfortunately, several side effects are reported, e.g. hypotension, nausea and vomiting (100-103). However, it might be interesting to use as a radioprotector during PSMA-TRT, but investigation is needed. Other examples of radioprotectors include bortezomib (protease inhibitor), HSP90 inhibitors, monosodium glutamate (MSG) and tempol (3, 93-95, 104-112).

In this study, the radioprotective effects of amifostine was investigated in prostate cancer and salivary gland cells following exposure to EBRT (X-rays). Functional damage to the salivary glands will be investigated on NKCC1 and AQP-5 protein expression via western blot. An alkaline phosphatase assay to determine the activity of the alkaline phosphatase enzyme will be conducted on PC3-Flu, PC3-PIP, and A-253 cells. Next, attempts will be made to generate an *in vitro* 3D model of the A-253 salivary gland cell line. The cytotoxicity of amifostine will be determined with a sulforhodamine B (SRB) based cytotoxicity assay, and the combinational effect on cell survival of EBRT and amifostine will be investigated via the MTS assay.

EXPERIMENTAL PROCEDURES

Cell culture - Human submandibular gland carcinoma A-253 cells were purchased from American Type Culture Collection (ATCC) and maintained in McCoy's 5A medium, supplemented with 10 % FBS and 1% penicillin-streptomycin. Human prostate cancer PC3-PIP (PSMA-positive) and PC3-Flu (PSMA-negative) cells were kindly provided by Dr. Pomper (John Hopkins University, Baltimore, USA). Cells were maintained in RPMI medium, supplemented with 10 % FBS, 1% penicillin-streptomycin and 2 µg/ml puromycin. All cell lines were maintained in an incubator at 37 °C with 5% CO_2. Cells were passaged when reaching around 80 % confluency.

3D culture - Wells of a 96 well plate (Greiner) were coated using 50 µl corning Matrigel® (356255) in concentrations of (0 %, 50 %, 75 % or 100 % (diluted in complete growth medium). The plate was then incubated for 30 min at 37 °C. Next, A-253 cells were plated at 5.000, 10.000 or 15.000 cells/well in triplicate. The plated cells were incubated at 37 °C for 30 min to allow cells to settle. Next, 60 µl of Matrigel®-McCoy 5A medium (in 1:10 dilution) was added to each well. Cells were cultured for 48 h, after which the medium was changed once every two days. Cell growth and formation of 3D structures were monitored using a Leica DMi1 microscope.

Protein lysate extraction - Total protein lysate was extracted from cells by adding 4 ml 0.25 % trypsin-EDTA solution and incubated for 3 min (for PC3-Flu and PC3-PIP cells) or 4 min (for A-253 cells) at 37 °C. Trypsin was inhibited by adding 8 ml complete growth medium, and the cells were centrifuged for 5 min at 200 x *g*. The pellet was dissolved in 1 ml PBS and centrifuged for 5 min at 200 x *g*. The pellet was resuspended in 200 µl RIPA buffer (supplemented with a phosphatase inhibitor tablet, P78420 and a protease inhibitor tablet, P78430) and sonicated for 30 sec with a TissueLyzer II (QIAGEN). Lastly, it was centrifuged in a cooled centrifuge for 10 min at 14.000 x *g*. Cell lysate was stored at -80 °C until further use. For the alkaline phosphatase assay, protein lysate was extracted by adding 4 ml 0.25 % trypsin-EDTA solution

and incubated for 3 min (for PC3-Flu and PC3-PIP cells) or 4 min (for A-253 cells) at 37 °C. Trypsin was inhibited by adding 8 ml complete growth medium, and the cells were centrifuged for 5 min at 450 x *g*. The pellet was dissolved in 1 ml PBS and centrifuged for 5 min at 450 x *g*. The pellet was resuspended in 125 µl CellLytic M reagent (C2978, supplemented with protease inhibitor (P8340, 1 premade tablet in 10 ml buffer). Cells were incubated for 15 min on a shaker and centrifuged for 15 min at 15.000 x *g*. Lysates were stored at -80 °C until further use. Protein concentrations were determined using a Bicinchoninic acid (BCA) protein assay kit (ThermoFisher), where 200 µl of BCA working reagent (BCA and $CuSO_4$ in 50:1 ratio) was added to 10 µl of the sample or standards with known protein concentrations. Absorbance was measured at 562 nm after 30 min incubation at 37 °C, and protein concentrations of the samples were calculated using a standard curve.

Western blot - Cell lysate of HK-2 cells was used as a negative control and A-549 as a positive control in optimization experiments. Detection of NKCC1 protein expression was optimized by loading 20, 40 or 60 µg protein which was heated for 10 min at 95 °C and loaded on an SDS-PAGE gel, and separated at 100 V for 10 min and 200 V for 30 min. The gel was transferred to a nitrocellulose membrane or PVDF membrane and blocked for 2 h using 5 % bovine serum albumin (BSA) + 0.05 % Tween-20 in TBST or 5 % nonfat dry milk (NFDM) + 0.05 % Tween-20 in TBS. Anti-NKCC1 rabbit polyclonal primary antibody (ThermoFisher, PA5-95145) was incubated overnight in different dilutions (1:1000, 1:2000, 1:5000), and secondary antibody goat-anti-rabbit HRP (Invitrogen, 65-6120) was incubated for 45 min at a concentration of 1:10000. The membrane was incubated with ECL substrate working solution (Bio-rad 170561) for 5 min, after which the membranes were imaged using a Fusion FX imager (ECL luminescence). A similar protocol was followed for the optimization of AQP-5 protein detection by western blot. Two different primary antibodies, anti-AQP-5 rabbit polyclonal antibody (Alomone, AQP-005 and Thermofisher, PA5-97290), were tested at different concentrations of the primary antibody (1/500, 1/1000, 1/2000 and 1/5000).

Alkaline phosphatase assay - Alkaline Phosphatase Diethanolamine Activity Kit (Sigma-Aldrich) was used to measure the alkaline phosphatase activity in PC3-Flu, PC3-PIP and A-253 lysate. Briefly, 196 µl of reaction buffer was added to the blank well of a 96-well plate, 192 µl of reaction buffer was added to the test sample wells and the control wells. 4 µl of 0.67M pNPP solution was added to each well, and the wells were equilibrated at 37 °C for 30 min. 4 µl test sample was added to the test well, and 4 µl alkaline phosphatase dilution (0.15 units/ml) was added to the control well. Absorbance was measured at 405 nm for 6 min. Alkaline phosphatase activity was calculated using the following equation:

$$\frac{\Delta A405\text{nm/ min test} - \Delta A405\text{nm/ min } Blank)\ (df)(Vf)}{(18.5)(Ve)}$$

Sulforhodamine B assay - Cytotoxicity of amifostine was measured with a sulforhodamine B (SRB) assay on PC3-Flu, PC3-PIP, and A-253 cells. Seeding densities are visualized in table 1. Cells were not passaged during experiments. After overnight incubation to allow cell attachment, 100 µl amifostine (0 , 10 , 50 , 100 , 200 or 1000 µM) was incubated for 1 h, 4 h or 16 h. Cells were fixed at 0, 1 and 5 days after treatment with 50 % trichloroacetic acid (TCA) solution, incubated for 1 h, washed and air-dried. SRB staining was performed by adding 50 µl 0.04 % sulforhodamine B solution and incubated for 20-30 min. Cells were washed with 1 % acetic acid until the unincorporated dye was removed

and the plates were left to dry. The incorporated dye was solubilized in 100 µl of Sulforhodamine B Assay solubilization buffer (10 mM Tris). Absorbance was measured at 565 nm and with a reference filter of 690 nm. Visualized data is normalized relative to the untreated control group.

Table 1: Seeding densities. Seeding density for the SRB and MTS assay for the PC3-Flu, PC3-PIP and A-253 cells. Numbers are expressed as cells/well.

Cell line	0h	1d	5d
PC3-Flu	10.000	6.000	3.000
PC3-PIP	10.000	6.000	3.000
A-253	15.000	6.000	5.000

Cell viability monitoring by MTS assay – PC3-Flu, PC3-PIP, and A-253 cells were seeded according to the same seeding densities as in the SRB assay (table 1). Cells were not passaged during experiments. After overnight incubation to allow cell attachment, cells were treated with 100 µl amifostine (0 , 10 , 50, 100, 200 or 1000 µM). Following 30 minutes incubation, cells were irradiated with 0, 2 or 5 Gy at <95 % confluence with a dose rate of 0.5 Gy/min, using an AGO HS320/250 X-ray cabinet. MTS assay was performed 0, 1 and 5 days after irradiation. The MTS assay was performed by adding 120 µl MTS reagent (1:6 dilution with complete growth medium). The absorbance was measured at 490 nm after 1 hour incubation for the A-253 cells and after 2 hours incubation for the PC3-Flu and PC3-PIP cells. The cell viability percentage was calculated and visualized data is normalized relative to the untreated control group.

Statistical analysis - Statistical analysis and graphs were made with GraphPad Prism 9. Comparison of groups was made via the Kruskall-Wallis test followed by Dunn's multiple comparison test. A significance level of 5 % was considered.

RESULTS

Initiating a 3D culture of A-253 salivary gland cells - Salivary gland A-253 cells were transformed from 2D to 3D using different concentrations (50 %, 75 % or 100 %) of the basement membrane matrix Matrigel®. 5.000, 10.000 or 15.000 cells/well were seeded. The cells treated with Matrigel® died prematurely, whereas a simultaneous 2D culture could be maintained. A structured pattern to minimize stress-inducing effects, such as reducing the time out of the incubator to a minimum was included during the second attempt. Here, cluster formation initiation was observed starting from day 3, which continued during the next few days. After 14 days, a limited number of clusters were detected. When comparing the cells treated with undiluted Matrigel®, 75 % diluted and 50 % diluted, it was observed that the transformation of the undiluted and 75 % diluted Matrigel® were the most adequate due to the size and speed of clump formation (figure 5). Also, it was observed that the lowest seeding density (5000 cells/well) is suboptimal. However, further optimization is warranted. Further cluster formation is needed. Also, the formation of acinar structures was missing.

Optimization of western blot conditions to detect NKCC1 and AQP-5 protein expression - NKCC1 and AQP-5 protein expression profiles were detected via western blot. HK-2 (human kidney cells, negative control) and A-549 cells (lung cancer cells, positive control) were included. For the detection of NKCC1 expression, 20, 40 and 60 µg of each protein lysate was loaded and both blocking with 5 % BSA + 0.05 % Tween-20 in TBST and with 5 % NFDM + 0.05 % Tween-20 in TBS was tested. Also, the difference between a nitrocellulose membrane and a PVDF membrane was tested. Lastly, different concentrations of primary antibody were tested (1/1000, 1/2000 and 1/5000). A band is

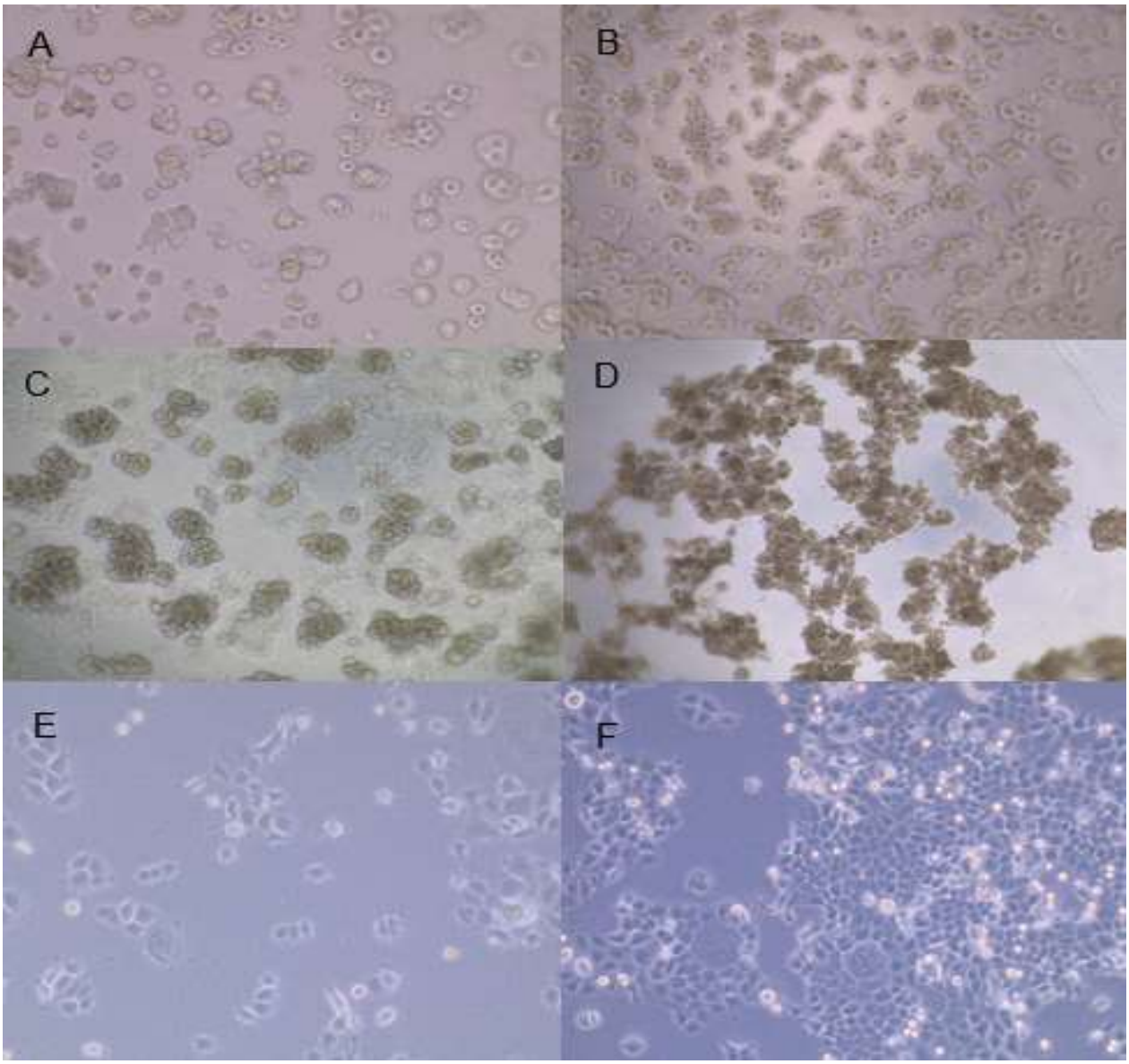

Figure 5: 3D culture of A-253 cells. (A) The cells started to grow in clusters from day 3. (B-C) The cluster formation continued in the next few days, day 4 (B) and day 7 (C). (D) After 14 days, the cells formed clusters of 3D cells that had grown to each other, as shown in the picture. (E-F) Pictures as a reference control of a 2D culture with (E) a low density and (F) a high density. All pictures are created with 100% Matrigel®. Images were taken using a Leica DMi1 microscope.

detected at approximately 130 kDa for the A549 cells, which is absent for the HK-2 cells (figure 6). When comparing the different concentrations of protein lysate loaded, it was clear that using 60 µg of protein lysate gave the clearest band (figure 6). Furthermore, it was chosen to proceed with 5 % BSA + 0.05 % Tween-20 in TBST to reduce non-specific binding. Also, it was opted to

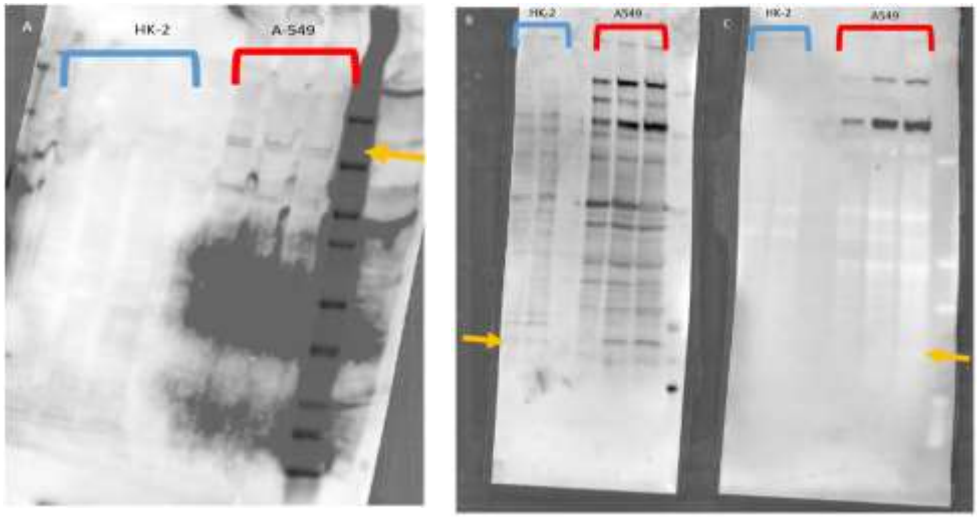

Figure 6: Western blot detection of NKCC1 and AQP-5 protein expression. (A) Detection of NKCC1 protein expression in A549, HK-2 (B) Detection of AQP-5 detection after blocking with 5% BSA + 0.05% Tween-20 in TBS and a primary antibody concentration of 1/500 in HK-2 and A549 cells. (c) Detection of AQP-5 after blocking with 5% NFDM + 0.05% Tween-20 in TBS and a primary antibody concentration of 1/1000 in HK-2 and A549 cells. The yellow line indicates the expected height of the band. Pictures taken with Fusion FX imager (ECL luminescence).

proceed with a nitrocellulose membrane due to the presence of non-specific background antibody binding on the PVDF membrane. Lastly, a 1/2000 dilution of the primary antibody gave clearest band (figure 6).

Optimization of AQP-5 protein expression detection was executed by loading different protein lysate concentrations (20, 40 and 60 µg) and testing different blocking buffers (5 % BSA + 0.05 % Tween-20 in TBST and 5 % NFDM + 0.05 % Tween-20 in TBST-), 2 different membranes (nitrocellulose and PVDF) and primary antibody concentrations (1/500, 1/1000, 1/2000 and 1/5000). Lastly, two antibodies were purchased from a different supplier. A band was expected around 35 kDa for both AQP-5 antibodies. However, no specific signal for AQP-5 could be detected due to the presence of background nonspecific antibody binding, so further optimization is needed (figure 6B and 6C).

Determination of alkaline phosphatase activity - Alkaline phosphatase (ALP) activity was measured with the Alkaline Phosphatase Diethanolamine Activity Kit in PC3-Flu, PC3-PIP, and A-253 cells (figure 7). A-253 cells had an ALP activity of $1.992*10^{-1}$ units/ml, while PC3-Flu cells had an ALP activity of $2.08*10^{-4}$ units/ml and PC3-PIP of $4.503*10^{-4}$ units/ml (figure 7). This indicates that A-253 cells had significantly more ALP activity than both PC3-Flu and PC3-PIP cells (p-value<0.0001). The difference in ALP activity between PC3-Flu and PC3-PIP was not statistically significant (p-value > 0.9999).

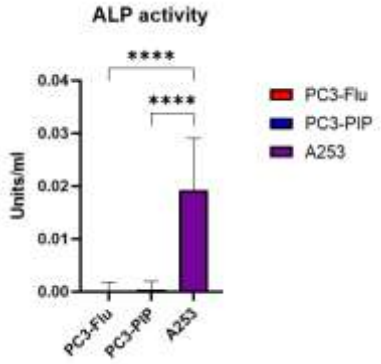

Figure 7: Alkaline phosphatase assay. The amount of alkaline phosphatase was measured in the PC3-Flu, PC3-PIP and A-253 cells. A-253 had a significantly higher amount of alkaline phosphatase activity compared to the PC3-Flu and PC3-PIP cells ($\alpha<0.05$). ****p-value<0.0001.

Cytotoxicity of amifostine in PC3-Flu and PC3-PIP prostate cancer and A-253 salivary gland cells. Cytotoxicity was determined with an SRB assay after incubation with different concentrations (0-1000 µM) of amifostine for 1, 4 or 16 hours. Cells were fixated 0, 1 or 5 days after treatment. The experiment was repeated twice with 3 biological replicates. Due to the high variance and a low number of replicates available, it was not possible to do statistical analysis. However, it is observed that the highest concentrations of amifostine seem to have a cytotoxic effect on the A-253 cells, as can be seen in the downward trend in figure 8. This is the case for the cells incubated with 200 µM and 1000 µM amifostine. This downward trend can be seen in most of the time points tested (figure 8). However, some results have biological variance, warranting further testing and optimization to produce repeatable results (Figure S1).

Similar treatment conditions were tested for the PC3-Flu and PC3-PIP cells and the same analyses was done. Here, comparable to the A-253 cells, a cytotoxic effect was detected by the downward trend for the highest concentrations of amifostine (200 µM and 1000 µM) (figure 8). Similar results were obtained for the different time points. However, biological variance was detected, so that no statistical analysis could be done (figure S2 and S3).

The protective effects of amifostine in PC3-Flu and PC3-PIP prostate cancer and A-253 salivary gland cells – A-253 cells were pretreated with amifostine (0-1000 µM). After 30 min, they were transferred to an irradiation facility and irradiated with 0, 2 or 5 Gy (X-rays). Cell viability was measured with an MTS assay after 0, 1 and 5 days. The experiment was performed twice, with 3 replicates each. Due to the high values of the control group for MTS(1d) and MTS(5d), it was chosen to proceed with the results of only 1 experiment, except for the results of MTS (0h). It can be observed that, immediately after treatment, no clear effect was visible for both the PC3-Flu, PC3-PIP and A-253 cells (figure 9). On the other hand, 1 and 5 days after treatment, reduced viability was detected for the highest concentrations of amifostine (200 µM and 1000 µM), as can be seen with the downward trend for these concentrations (figure 9), which is in line with the results from the SRB assay (figure 8). Contrary, an increasing trend is detected for some concentrations of amifostine (10 µM, 50 µM and 100 µM), compared to the untreated control group (figure 9). Some other graphs contain biological variance, making them difficult to interpret corretly (figure 9).

DISCUSSION

Initiating a 3D culture of A-253 salivary gland cells - In order to investigate the uptake mechanisms by the salivary glands, a reliable model is needed (3). To try to get an *in vivo* like model, it was opted to develop a 3D cell culture model of the A-253 salivary glands. This is more reliable compared to a 2D model due to the

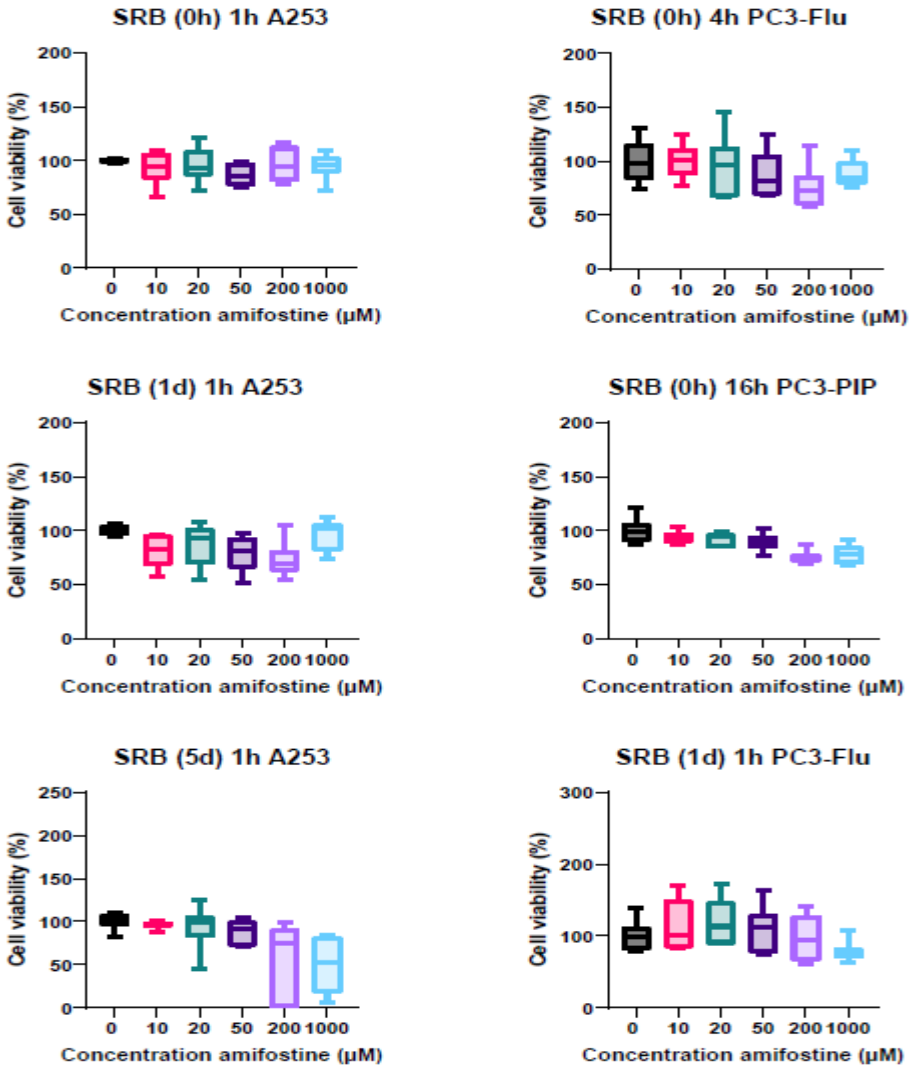

Figure 8: Cytotoxicity of amifostine in PC3-Flu, PC3-PIP and A-253 cells . Cytotoxicity after incubation with amifostine for 1, 4 or 16 hours. Cells were fixated after 0, 1 or 5 days with different concentrations of amifostine. All results are normalized to the untreated cells. Some examples are visualized, other graphs in the supplementals (S1-S3). N=6

connections with other cells and the formation of acinar and ductal structures in 3D cultures (113-116). A higher expression of functional proteins like AQP-5 and NKCC1 is expected in a 3D culture, allowing detection of functional damage by analyzing the differences in expression profiles (113). In order to achieve this, a 2D culture of the A-253 cells was transformed into a 3D culture by using the basement membrane preparation, Matrigel®, which has previously been successfully used for this cell line (113). The cells started to grow in clusters which was in line with previous reports (113, 117, 118). However, some optimization is needed by searching for the optimal Matrigel® concentration and seeding density. The formation of a honeycomb network

was expected at 3 hours, based on literature (113). Also, the formation of multilobular structures was expected at 48 hours, and the formation of acinar structures was expected at 72 hours (113).

The inconsistent formation of 3D clusters can have multiple explanations. In the first attempt, the time spent outside the incubator for imaging was substantial (119). This time was reduced during the second attempt. Next, partial thawing of the Matrigel® stock solution might have altered protein components, resulting in ineffective formation of 3D cultures (120, 121). Using a 24-well plate, together with a higher seeding density might be better compared to the limited space available in a 96-well plate (113). Another possibility is the use of Geltrex™ instead of Matrigel®, which is also proven to be effective in transforming a 2D to a 3D culture and more importantly, easier to use in practice (122, 123). However, due to the limited time available and logistic problems (unavailability and long delivery time of Matrigel®), it was not possible to proceed with culturing of the 3D cell culture in Geltrex™. In future experiments, evaluation of cluster formation can be performed with immunostaining and confocal microscopy. An even more appropriate *in vitro* model could be the use of salivary gland organoids. Here different cell lines are combined in an organ like structure, with addition of functional tissue like structures. Organoids will better represent the

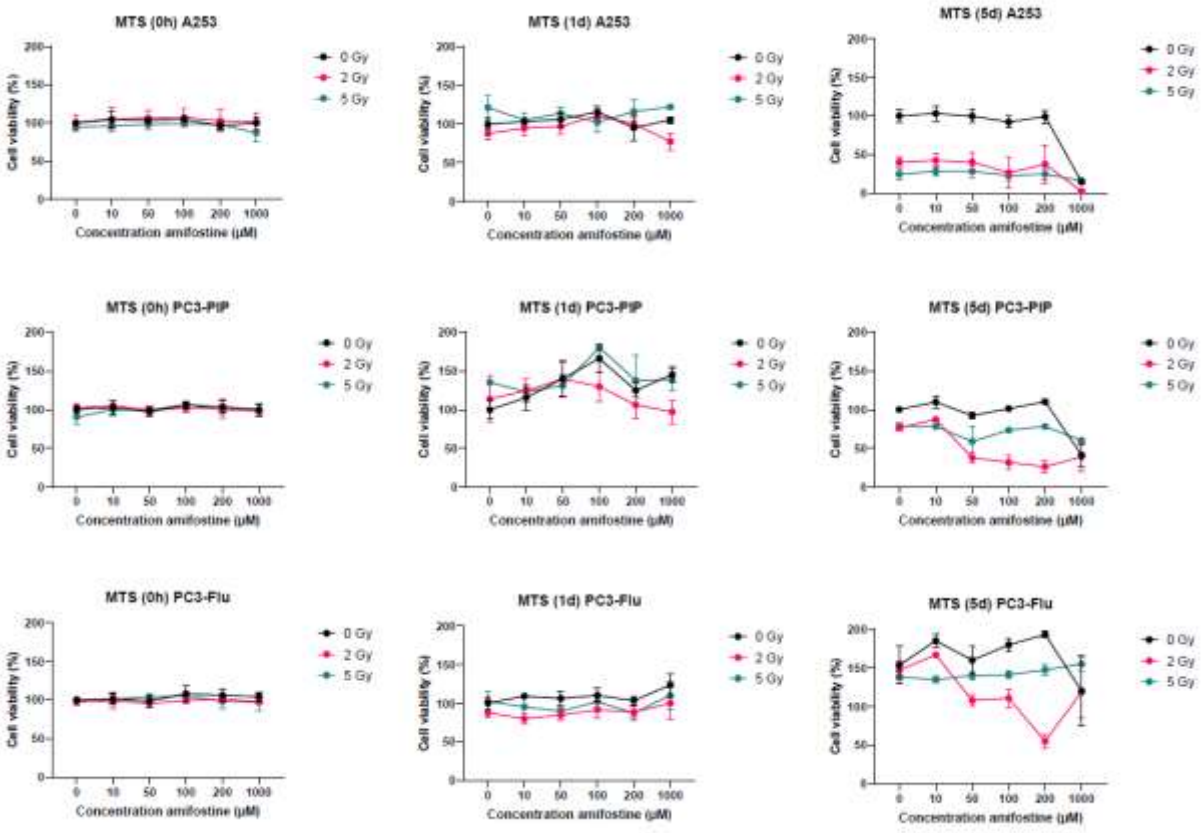

Figure 9: The protective effect of amifostine during EBRT on PC3-Flu, PC3-PIP and A-253 cells . Cells were incubated with amifostine (0-1000 µM) for 30 min. Cell viability was measured 0 day, 1 day or 5 days after exposure to 0, 2 or 5 Gy. N=6 for SRB(0h) and N=3 for SRB(1d) and SRB(5d).

microenvironment and architecture, but they are more difficult to create and maintain (124, 125).

Optimization of western blot conditions to detect NKCC1 and AQP-5 protein expression. NKCC1 and AQP-5 protein expression of 2D cultures was optimized in A-549 lung cancer and HK-2 human kidney cells (figure 6. The choice for NKCC1 and AQP-5 protein detection was based on their importance in the secretion of saliva since saliva secretion is disrupted after exposure to EBRT or PSMA-TRT (91, 92, 126). Positive (A-549) and negative (HK-2) cell lines were included based on findings in the literature (90, 127-130). NKCC1 protein expression was detected at 130 kDa in A-549 but was absent in HK-2 cells, confirming literature reports (90, 127-133). The optimized protocol can be further used to detect the presence of NKCC1 in PC3-Flu, PC3-PIP and A-253 cells.

Another protein under investigation is AQP-5. Attempts were made to optimize western blot protein detection. AQP-5 has an approximate molecular weight of 35 kDa, based on literature (134-137). Different conditions were used, loading different protein lysate concentrations (20, 40, 60 µg) and testing different blocking buffers (5 % BSA + 0.05 % Tween-20 in TBST and 5 % NFDM + 0.05 % Tween-20 in TBST-), 2 different membranes (nitrocellulose and PVDF) and primary antibody concentrations (1/500, 1/1000, 1/2000 and 1/5000). Lastly, two antibodies were purchased from different suppliers, but nonspecific binding remained high, rendering it impossible to quantify specific AQP-5 expression (figure 6). A possible solution might be to include antigen retrieval with citrate solution (0.01 M, pH 6.0, (138)). Here, the membrane is incubated with a citrate buffer, which is thought to improve protein signal by increasing the band density. Incubation with citrate solution will expose the antigen-binding sites, which can increase the amount of antibody/epitope interaction (13, 139-143). Another option includes lowering the concentration of NFDM or BSA blocking buffers to 1 % (144).

After optimization of both NKCC1 and AQP-5 protein expression via western blot and the creation of a successful 3D culture of the A-253 cells, these results can be compared between the 2D and 3D culture, followed by analysis before and after exposure to external radiation, and later after exposure to [^{177}Lu]Lu-PSMA-617 therapy. Next, protein expression can be quantified, after which the effect of the transformation of 2D to 3D, external radiotherapy and [^{177}Lu]Lu-PSMA-617 therapy on NKCC1 expression can be evaluated. In this way, the effect on important channels for saliva secretion and thus functional damage can be estimated.

Determination of alkaline phosphatase activity - Amifostine is FDA approved as a radioprotector during EBRT treatment for head- and neck cancer (figure 4) (66, 67, 93, 94, 97). Since alkaline phosphatase is needed for the conversion of amifostine to its active thiol metabolite, the presence of alkaline phosphatase was measured in the different cell lines (3, 93). A-253 cells have a higher alkaline phosphatase activity compared to PC3-Flu and PC3-PIP cells (p-value < 0.0001). This is of high importance for the use of amifostine as a radioprotector in combination with [^{177}Lu]Lu-PSMA-617 therapy (145). Since alkaline phosphatase is downregulated in cancer cells, cancer cells will benefit less from amifostine compared to healthy cells (3, 93). These results indicate that treating prostate cancer with [^{177}Lu]Lu-PSMA-617 therapy potentially can benefit of co-administration of amifostine in terms of salivary gland toxicity.

Cytotoxicity of amifostine in PC3-Flu and PC3-PIP prostate cancer and A-253 salivary gland cells - The cytotoxicity of amifostine was tested by treatment of cells with increasing concentrations of amifostine (0 – 1000 µM). Furthermore, the optimal treatment concentration was determined. Other research has shown cytotoxic effects of amifostine by inducing apoptosis and affecting p53 expression, 5 days after exposure to 20 µM amifostine (146). However, this was in a myelodysplastic syndromes cell line, so further investigation of the effect on PC3-Flu, PC3-PIP and A-253 cells is needed.

The results from the SRB assays indicated that there is no effect of amifostine on the cell viability of A-253 cells immediately after treatment. Both the incubation period with amifostine and the time after treatment must be long enough to ensure the conversion of amifostine to its active metabolite (98, 99, 102, 147). This could explain the results for the assays with only one hour of incubation with amifostine and those which were fixated immediately or 1 day after treatment. However, signs of cytotoxicity were observed 5 days after treatment with the highest concentrations of amifostine (200 µM and 1000 µM). Unfortunately, a lot of variance was detected for some results of 1 and 5 days. An explanation for the biological variance is that, in some wells, the distribution of cells was inhomogenous (more in the middle). Optimization is needed to spread the cells evenly and enable uniform staining. This can be achieved by adding the cell suspension directly to the bottom of the well while avoiding touching the walls. Furthermore, a short spin of the plate might improve the results (148). Lastly, the protocol was followed according to the manufacturer (SigmaAldrich). Nevertheless, this protocol was optimized with uveal melanoma cell lines (149). It is possible that those cells have other characteristics compared to the cells used. This indicates that further optimization is needed to create a dose-response curve to determine which concentration of amifostine would be optimal for the protection of the salivary glands without being cytotoxic (150). This dose-response curve can be created by testing different concentrations. Also, repeating the tested concentrations is needed for confirmation of the results due to the limited number of replicates (n=6).

The cytotoxicity on PC3-Flu and PC3-PIP cells was also investigated, expecting that amifostine will not have a big influence on PC3-Flu and PC3-PIP cells due to the absence of alkaline phosphatase activity (3, 93). However, too much variation was present between the results, so optimization is needed. This variance can partly be explained by the high values of multiple control wells (only medium). The high values of the controls have a big impact on the results by correcting for the presence of proteins in the medium (148). So optimization of the control group is needed. Another solution to reduce this variation is the optimization of the seeding density, which is determined by the doubling time of the cell line and the size of the cells (148). Ideally, cells should be around 90 % confluent at the end of the experiment (148, 151). This number is a critical step that determines the proliferation capacity of a group of cells. Also, the presence of air bubbles might affect the acquiring and must be avoided (148, 150).

Another critical step is the addition of fixative (TCA solution). This must be added gently. Otherwise, the cells may dislodge (148, 152). Focusing on the gentle addition of TCA solution or overnight incubation with TCA solution might reduce inter-well variability (148, 152). Also, using 10 % TCA instead of 50 % might improve the results (150). Another possibility is using another fixative (such as paraformaldehyde).

Removing the medium while leaving only the minimal amount of medium (10 µl) before adding TCA solution might reduce variability (153). Due to the adherent character of the cells, it is not expected that this will affect the number of cells (152, 153). Further, it is possible to stain with 0,1 % SRB in 1% acetic acid instead to improve the staining quality (154).

The protective effects of amifostine in PC3-Flu and PC3-PIP prostate cancer and A-253 salivary gland cells - Following the SRB assay, an MTS assay was performed to investigate the combinational effect of amifostine and external beam radiation (X-rays). The same concentrations of amifostine were tested as in the SRB assay (0, 10, 20, 50, 200 and 1000 µM). Cell viability was measured 0, 1 or 5 days after exposure to 0, 2 or 5 Gy X-rays (155-157). Unfortunately, the values of the blanc wells of the first experiment were high, resulting in negative results for 1 and 5 days after treatment. Further, variance was detected between the results of the first and the second experiment. Because of this, it was decided to proceed with the results for the second experiment only for 1 and 5 days. No clear protecting effect of amifostine was visible after treatment with EBRT on the A-253 cells (figure 8), which is counterintuitive, as the A-253 cells should have alkaline phosphatase to convert amifostine to the active thiol metabolite (96, 158). The same optimization as mentioned above is needed for the MTS assay. It is expected that an increasing concentration of amifostine will result in a decreasing toxic effect of the EBRT for the A-253 cells, as also mentioned in literature (159, 160). But, this beneficial effect will decrease when using the highest concentrations of amifostine (200 µM and 1000 µM), as mentioned in the SRB assay above (146, 158). Also, using another cell line might be a solution. It was chosen to work with A-253 cells, which are derived from a human salivary gland epidermoid carcinoma (161). This choice was based on literature showing the formation of acinar structures (rounded secretory units) in a 3D cell model (113). But, as these cells are derived from cancer tissue, it is possible that their alkaline phosphatase activity is insufficient to convert amifostine to its active thiol metabolite. As mentioned above, it was seen that the ALP activity of the A-253 cells was higher compared to the PC3-Flu and PC3-PIP cells, but a comparison with healthy cells is missing and might be needed. An alternative cell line that might be useful is Hs 917.T, derived from a human parotid salivary gland, since they also have proven to be effective for the transformation of a 3D culture and have a benign origin (162, 163). However, limited studies have been performed using these cells, and cultivation remains challenging.

The beneficial effect of amifostine is not expected to be present in the PC3-Flu and PC3-PIP cells due to the downregulation of alkaline phosphatase (159, 160). This effect is also seen in other types of cancer cells, e.g. human non-small cell lung cancer cells or mice (159, 160). Further investigation of the combinational effect of EBRT and amifostine is needed. This can be done by testing cumulative doses instead. Exposure to 2 and 5 Gy was chosen based on literature, but testing other doses can be useful (66, 76, 164). Also, optimization of the incubation time of amifostine before treatment with EBRT is needed. It is possible that the 30 min incubation period is too short. This should be long enough to ensure that the healthy cells have had enough time to convert amifostine to its active thiol metabolite to make sure that the active radioprotector itself is present in the cells. The time point of 30 min was chosen based on the literature (98, 99, 102, 147). Lastly, adding an extra time point such as 10 days might be interesting. This can be explained by the high fractionation sensitivity of prostate cancer

cells (low α/β ratio, comparable to healthy tissue). This low ratio will cause a late onset of cytotoxic effects (165-168). Additionally, other in-house research observed an increase of metabolic activity in the first hours after treatment with radiotherapy, which is in a later stage decreased due to cell death. Also, other research has shown metabolic alterations in cells after exposure to radiation. This alteration depends on numerous characteristics e.g. tumor volume and location (169, 170). Since the MTS assay is based on metabolic activity, this might influence the results 0 and 1 day after treatment. This might be solved by using another assay to measure cell viability, such as the live and dead cell assay (171).

CONCLUSION

The first steps of the formation of a 3D salivary gland A-253 culture succeeded. Further optimization is needed to create adequate acinar structures and provoke changes in the protein expression profile. NKCC1 protein expression detection by western blot was successfully optimized. For the detection of AQP-5, further optimization is needed. Signs of cytotoxicity are detected with the SRB assay at higher amifostine concentrations, but replication is needed. No conclusion can be drawn from the protective effect of amifostine during EBRT due to inconclusive results.

REFERENCES

1. Ferlay J, Colombet M, Soerjomataram I, Dyba T, Randi G, Bettio M, et al. Cancer incidence and mortality patterns in Europe: Estimates for 40 countries and 25 major cancers in 2018. Eur J Cancer. 2018;103:356-87.
2. Culp MB, Soerjomataram I, Efstathiou JA, Bray F, Jemal A. Recent Global Patterns in Prostate Cancer Incidence and Mortality Rates. Eur Urol. 2020;77(1):38-52.
3. Heynickx N, Herrmann K, Vermeulen K, Baatout S, Aerts A. The salivary glands as a dose limiting organ of PSMA- targeted radionuclide therapy: A review of the lessons learnt so far. Nucl Med Biol. 2021;98-99:30-9.
4. Grozescu T, Popa F. Prostate cancer between prognosis and adequate/proper therapy. J Med Life. 2017;10(1):5-12.
5. Giona S. The Epidemiology of Prostate Cancer. In: Bott SRJ, Ng KL, editors. Prostate Cancer. Brisbane (AU)2021.
6. Sung H, Ferlay J, Siegel RL, Laversanne M, Soerjomataram I, Jemal A, et al. Global Cancer Statistics 2020: GLOBOCAN Estimates of Incidence and Mortality Worldwide for 36 Cancers in 185 Countries. CA Cancer J Clin. 2021;71(3):209-49.
7. Schatten H. Brief Overview of Prostate Cancer Statistics, Grading, Diagnosis and Treatment Strategies. Adv Exp Med Biol. 2018;1095:1-14.
8. Prostate Cancer American Cancer Society [Available from: https://www.cancer.org/cancer/prostate-cancer.html.
9. Nguyen-Nielsen M, Borre M. Diagnostic and Therapeutic Strategies for Prostate Cancer. Semin Nucl Med. 2016;46(6):484-90.
10. Chang AJ, Autio KA, Roach M, 3rd, Scher HI. High-risk prostate cancer-classification and therapy. Nat Rev Clin Oncol. 2014;11(6):308-23.
11. Siegel DA, O'Neil ME, Richards TB, Dowling NF, Weir HK. Prostate Cancer Incidence and Survival, by Stage and Race/Ethnicity - United States, 2001-2017. MMWR Morb Mortal Wkly Rep. 2020;69(41):1473-80.
12. Kirby M, Hirst C, Crawford ED. Characterising the castration-resistant prostate cancer population: a systematic review. Int J Clin Pract. 2011;65(11):1180-92.
13. Garcia JA, Rini BI. Castration-resistant prostate cancer: many treatments, many options,

many challenges ahead. Cancer. 2012;118(10):2583-93.
14. Komura K, Sweeney CJ, Inamoto T, Ibuki N, Azuma H, Kantoff PW. Current treatment strategies for advanced prostate cancer. Int J Urol. 2018;25(3):220-31.
15. Silver DA, Pellicer I, Fair WR, Heston WD, Cordon-Cardo C. Prostate-specific membrane antigen expression in normal and malignant human tissues. Clin Cancer Res. 1997;3(1):81-5.
16. Juzeniene A, Stenberg VY, Bruland OS, Larsen RH. Preclinical and Clinical Status of PSMA-Targeted Alpha Therapy for Metastatic Castration-Resistant Prostate Cancer. Cancers (Basel). 2021;13(4).
17. Czerwinska M, Bilewicz A, Kruszewski M, Wegierek-Ciuk A, Lankoff A. Targeted Radionuclide Therapy of Prostate Cancer-From Basic Research to Clinical Perspectives. Molecules. 2020;25(7).
18. Hofman MS, Hicks RJ, Maurer T, Eiber M. Prostate-specific Membrane Antigen PET: Clinical Utility in Prostate Cancer, Normal Patterns, Pearls, and Pitfalls. Radiographics. 2018;38(1):200-17.
19. Farag M, Bolton D, Lawrentschuk N. Prostate-specific membrane antigen for the surgical oncologist: interpreting expression beyond the prostate. ANZ J Surg. 2020;90(5):715-8.
20. Chang SS. Overview of prostate-specific membrane antigen. Rev Urol. 2004;6 Suppl 10:S13-8.
21. Mahadevan D, Saldanha JW. The extracellular regions of PSMA and the transferrin receptor contain an aminopeptidase domain: implications for drug design. Protein Sci. 1999;8(11):2546-9.
22. Rajasekaran AK, Anilkumar G, Christiansen JJ. Is prostate-specific membrane antigen a multifunctional protein? Am J Physiol Cell Physiol. 2005;288(5):C975-81.
23. Davis MI, Bennett MJ, Thomas LM, Bjorkman PJ. Crystal structure of prostate-specific membrane antigen, a tumor marker and peptidase. Proc Natl Acad Sci U S A. 2005;102(17):5981-6.
24. Liu H, Rajasekaran AK, Moy P, Xia Y, Kim S, Navarro V, et al. Constitutive and antibody-induced internalization of prostate-specific membrane antigen. Cancer Res. 1998;58(18):4055-60.
25. Kratochwil C, Giesel FL, Eder M, Afshar-Oromieh A, Benesova M, Mier W, et al. [(1)(7)(7)Lu]Lutetium-labelled PSMA ligand-induced remission in a patient with metastatic prostate cancer. Eur J Nucl Med Mol Imaging. 2015;42(6):987-8.
26. Winter G, Vogt A, Jimenez-Franco LD, Rinscheid A, Yousefzadeh-Nowshahr E, Solbach C, et al. Modelling the internalisation process of prostate cancer cells for PSMA-specific ligands. Nucl Med Biol. 2019;72-73:20-5.
27. Ferdinandus J, Violet J, Sandhu S, Hofman MS. Prostate-specific membrane antigen theranostics: therapy with lutetium-177. Curr Opin Urol. 2018;28(2):197-204.
28. Wang F, Li Z, Feng X, Yang D, Lin M. Advances in PSMA-targeted therapy for prostate cancer. Prostate Cancer Prostatic Dis. 2021.
29. Sheremeta MS, Trukhin AA, Korchagina MO. [The use of radioactive substances in medicine - history and development prospects]. Probl Endokrinol (Mosk). 2021;67(6):59-67.
30. Obaldo JM, Hertz BE. The early years of nuclear medicine: A Retelling. Asia Ocean J Nucl Med Biol. 2021;9(2):207-19.
31. Types of ionizing radiation Mirion Technologies [Available from: https://www.mirion.com/learning-center/radiation-safety-basics/types-of-ionizing-radiation.
32. Sollini M, Marzo K, Chiti A, Kirienko M. The five "W"s and "How" of Targeted Alpha

Therapy: Why? Who? What? Where? When? and How? Rend Lincei-Sci Fis. 2020;31(2):231-47.
33. De Vincentis G, Gerritsen W, Gschwend JE, Hacker M, Lewington V, O'Sullivan JM, et al. Advances in targeted alpha therapy for prostate cancer. Ann Oncol. 2019;30(11):1728-39.
34. Aghevlian S, Boyle AJ, Reilly RM. Radioimmunotherapy of cancer with high linear energy transfer (LET) radiation delivered by radionuclides emitting alpha-particles or Auger electrons. Adv Drug Deliv Rev. 2017;109:102-18.
35. Feuerecker B, Tauber R, Knorr K, Heck M, Beheshti A, Seidl C, et al. Activity and Adverse Events of Actinium-225-PSMA-617 in Advanced Metastatic Castration-resistant Prostate Cancer After Failure of Lutetium-177-PSMA. Eur Urol. 2021;79(3):343-50.
36. Qin Y, Imobersteg S, Blanc A, Frank S, Schibli R, Behe MP, et al. Evaluation of Actinium-225 Labeled Minigastrin Analogue [(225)Ac]Ac-DOTA-PP-F11N for Targeted Alpha Particle Therapy. Pharmaceutics. 2020;12(11).
37. Morgenstern A, Apostolidis C, Kratochwil C, Sathekge M, Krolicki L, Bruchertseifer F. An Overview of Targeted Alpha Therapy with (225)Actinium and (213)Bismuth. Curr Radiopharm. 2018;11(3):200-8.
38. Welsh JS. Beta radiation. Oncologist. 2006;11(2):181-3.
39. Jodal L. Beta emitters and radiation protection. Acta Oncol. 2009;48(2):308-13.
40. Asadian S, Mirzaei H, Kalantari BA, Davarpanah MR, Mohamadi M, Shpichka A, et al. beta-radiating radionuclides in cancer treatment, novel insight into promising approach. Pharmacol Res. 2020;160:105070.
41. Waksman R, Raizner A, Popma JJ. Beta emitter systems and results from clinical trials. state of the art. Cardiovasc Radiat Med. 2003;4(2):54-63.
42. Pan MH, Gao DW, Feng J, He J, Seo Y, Tedesco J, et al. Biodistributions of 177Lu- and 111In-labeled 7E11 antibodies to prostate-specific membrane antigen in xenograft model of prostate cancer and potential use of 111In-7E11 as a pre-therapeutic agent for 177Lu-7E11 radioimmunotherapy. Mol Imaging Biol. 2009;11(3):159-66.
43. Sartor O, de Bono J, Chi KN, Fizazi K, Herrmann K, Rahbar K, et al. Lutetium-177-PSMA-617 for Metastatic Castration-Resistant Prostate Cancer. N Engl J Med. 2021;385(12):1091-103.
44. Cancer Stat Facts: Prostate Cancer National Cancer Institute [Available from: https://seer.cancer.gov/statfacts/html/prost.html.
45. Morris MJ, De Bono JS, Chi KN, Fizazi K, Herrmann K, Rahbar K, et al. Phase III study of lutetium-177-PSMA-617 in patients with metastatic castration-resistant prostate cancer (VISION). J Clin Oncol. 2021;39(18).
46. FDA approves Pluvicto for metastatic castration-resistant prostate cancer US Food&drug administration [Available from: https://www.fda.gov/drugs/resources-information-approved-drugs/fda-approves-pluvicto-metastatic-castration-resistant-prostate-cancer.
47. Marion JB. Physics in the Modern World - 21 - Radiation - Effects and uses. ScienceDirect1981.
48. Sanchez-Crespo A, Jussing E, Bjorklund AC, Pokrovskaja Tamm K. Hallmarks in prostate cancer imaging with Ga68-PSMA-11-PET/CT with reference to detection limits and quantitative properties. EJNMMI Res. 2018;8(1):27.
49. Singh B, Sharma S, Bansal P, Hooda M, Singh H, Parihar AS, et al. Comparison of the diagnostic utility of 99mTc-PSMA scintigraphy versus 68Ga-PSMA-11 PET/CT in the detection

of metastatic prostate cancer and dosimetry analysis: a gamma-camera-based alternate prostate-specific membrane antigen imaging modality. Nucl Med Commun. 2021;42(5):482-9.
50. Persson L. The Auger electron effect in radiation dosimetry. Health Phys. 1994;67(5):471-6.
51. Buchegger F, Perillo-Adamer F, Dupertuis YM, Delaloye AB. Auger radiation targeted into DNA: a therapy perspective. Eur J Nucl Med Mol Imaging. 2006;33(11):1352-63.
52. Radchenko V, Engle JW, Thisgaard H. Status and future perspectives of Meitner-Auger and low energy electron-emitting radionuclides for targeted radionuclide therapy. Nucl Med Biol. 2021;94-95:106.
53. Kiess AP, Minn I, Chen Y, Hobbs R, Sgouros G, Mease RC, et al. Auger Radiopharmaceutical Therapy Targeting Prostate-Specific Membrane Antigen. J Nucl Med. 2015;56(9):1401-7.
54. Shen CJ, Minn I, Hobbs RF, Chen Y, Josefsson A, Brummet M, et al. Auger radiopharmaceutical therapy targeting prostate-specific membrane antigen in a micrometastatic model of prostate cancer. Theranostics. 2020;10(7):2888-96.
55. Cornelissen B, Vallis KA. Targeting the nucleus: an overview of Auger-electron radionuclide therapy. Curr Drug Discov Technol. 2010;7(4):263-79.
56. Makrigiorgos G, Adelstein SJ, Kassis AI. Auger electron emitters: insights gained from in vitro experiments. Radiat Environ Biophys. 1990;29(2):75-91.
57. Ku A, Facca VJ, Cai Z, Reilly RM. Auger electrons for cancer therapy - a review. EJNMMI Radiopharm Chem. 2019;4(1):27.
58. Khreish F, Ghazal Z, Marlowe RJ, Rosar F, Sabet A, Maus S, et al. 177 Lu-PSMA-617 radioligand therapy of metastatic castration-resistant prostate cancer: Initial 254-patient results from a prospective registry (REALITY Study). Eur J Nucl Med Mol Imaging. 2022;49(3):1075-85.
59. Iravani A, Violet J, Azad A, Hofman MS. Lutetium-177 prostate-specific membrane antigen (PSMA) theranostics: practical nuances and intricacies. Prostate Cancer Prostatic Dis. 2020;23(1):38-52.
60. Klein Nulent TJW, van Es RJJ, Willems SM, Braat A, Devriese LA, de Bree R, et al. First experiences with (177)Lu-PSMA-617 therapy for recurrent or metastatic salivary gland cancer. EJNMMI Res. 2021;11(1):126.
61. Ahmadzadehfar H, Eppard E, Kurpig S, Fimmers R, Yordanova A, Schlenkhoff CD, et al. Therapeutic response and side effects of repeated radioligand therapy with 177Lu-PSMA-DKFZ-617 of castrate-resistant metastatic prostate cancer. Oncotarget. 2016;7(11):12477-88.
62. Junqueira MZ, Rocha NH, Sapienza MT. (68)Ga-PSMA PET/CT: effect of external cooling on salivary gland uptake. Radiol Bras. 2021;54(3):171-6.
63. Wollenweber T, Zisser L, Kretschmer-Chott E, Weber M, Grubmuller B, Kramer G, et al. Renal and Salivary Gland Functions after Three Cycles of PSMA-617 Therapy Every Four Weeks in Patients with Metastatic Castration-Resistant Prostate Cancer. Curr Oncol. 2021;28(5):3692-704.
64. Rosar F, Kochems N, Bartholoma M, Maus S, Stemler T, Linxweiler J, et al. Renal Safety of [(177)Lu]Lu-PSMA-617 Radioligand Therapy in Patients with Compromised Baseline Kidney Function. Cancers (Basel). 2021;13(12).
65. Yordanova A, Becker A, Eppard E, Kurpig S, Fisang C, Feldmann G, et al. The impact of repeated cycles of radioligand therapy using [(177)Lu]Lu-PSMA-617 on renal function in patients with hormone refractory metastatic prostate cancer. Eur J Nucl Med Mol Imaging. 2017;44(9):1473-9.

66. Grundmann O, Mitchell GC, Limesand KH. Sensitivity of salivary glands to radiation: from animal models to therapies. J Dent Res. 2009;88(10):894-903.
67. Dirix P, Nuyts S, Van den Bogaert W. Radiation-induced xerostomia in patients with head and neck cancer: a literature review. Cancer. 2006;107(11):2525-34.
68. Klein Nulent TJW, Valstar MH, de Keizer B, Willems SM, Smit LA, Al-Mamgani A, et al. Physiologic distribution of PSMA-ligand in salivary glands and seromucous glands of the head and neck on PET/CT. Oral Surg Oral Med Oral Pathol Oral Radiol. 2018;125(5):478-86.
69. Valstar MH, Owers EC, Al-Mamgani A, Smeele LE, van de Kamer JB, Sonke JJ, et al. Prostate-specific membrane antigen positron emission tomography/computed tomography as a potential tool to assess and guide salivary gland irradiation. Phys Imaging Radiat Oncol. 2019;9:65-8.
70. Rupp NJ, Umbricht CA, Pizzuto DA, Lenggenhager D, Topfer A, Muller J, et al. First Clinicopathologic Evidence of a Non-PSMA-Related Uptake Mechanism for (68)Ga-PSMA-11 in Salivary Glands. J Nucl Med. 2019;60(9):1270-6.
71. Salivary Glands Anatomy Memorial Sloan Kettering Cancer Center [Available from: https://www.mskcc.org/.
72. Valstar MH, de Bakker BS, Steenbakkers RJHM, de Jong KH, Smit LA, Nulent TJWK, et al. The tubarial salivary glands: A potential new organ at risk for radiotherapy. Radiother Oncol. 2021;154:292-8.
73. Silvers AR, Som PM. Salivary glands. Radiol Clin North Am. 1998;36(5):941-66, vi.
74. Barrows CML, Wu D, Farach-Carson MC, Young S. Building a Functional Salivary Gland for Cell-Based Therapy: More than Secretory Epithelial Acini. Tissue Eng Part A. 2020;26(23-24):1332-48.
75. Konings AW, Coppes RP, Vissink A. On the mechanism of salivary gland radiosensitivity. Int J Radiat Oncol Biol Phys. 2005;62(4):1187-94.
76. Avila JL, Grundmann O, Burd R, Limesand KH. Radiation-induced salivary gland dysfunction results from p53-dependent apoptosis. Int J Radiat Oncol Biol Phys. 2009;73(2):523-9.
77. Peter B, Van Waarde MA, Vissink A, s-Gravenmade EJ, Konings AW. The role of secretory granules in the radiosensitivity of rat salivary gland acini--a morphological study. Radiat Res. 1994;140(3):419-28.
78. Radfar L, Sirois DA. Structural and functional injury in minipig salivary glands following fractionated exposure to 70 Gy of ionizing radiation: an animal model for human radiation-induced salivary gland injury. Oral Surg Oral Med Oral Pathol Oral Radiol Endod. 2003;96(3):267-74.
79. Henriksson R, Frojd O, Gustafsson H, Johansson S, Yi-Qing C, Franzen L, et al. Increase in mast cells and hyaluronic acid correlates to radiation-induced damage and loss of serous acinar cells in salivary glands: the parotid and submandibular glands differ in radiation sensitivity. Br J Cancer. 1994;69(2):320-6.
80. Aggarwal S, Ricklis RM, Williams SA, Denmeade SR. Comparative study of PSMA expression in the prostate of mouse, dog, monkey, and human. Prostate. 2006;66(9):903-10.
81. Rovenska M, Hlouchova K, Sacha P, Mlcochova P, Horak V, Zamecnik J, et al. Tissue expression and enzymologic characterization of human prostate specific membrane antigen and its rat and pig orthologs. Prostate. 2008;68(2):171-82.
82. Svajdova M, Kazda T, Dubinsky P, Slampa P. Radical external beam reirradiation of

recurrent head and neck cancer. Klin Onkol. 2021;34(2):103-12.
83. Delaney G, Jacob S, Barton M. Estimation of an optimal external beam radiotherapy utilization rate for head and neck carcinoma. Cancer. 2005;103(11):2216-27.
84. Fox PC. Acquired salivary dysfunction. Drugs and radiation. Ann N Y Acad Sci. 1998;842:132-7.
85. Bourry N, Guy N, Achard JL, Verrelle P, Clavelou P, Lapeyre M. Salivary glands radiotherapy to reduce sialorrhea in amyotrophic lateral sclerosis: dose and energy. Cancer Radiother. 2013;17(3):191-5.
86. Ortholan C, Benezery K, Bensadoun RJ. [Normal tissue tolerance to external beam radiation therapy: salivary glands]. Cancer Radiother. 2010;14(4-5):290-4.
87. Ship JA, Hu K. Radiotherapy-induced salivary dysfunction. Semin Oncol. 2004;31(6 Suppl 18):29-36.
88. Hawkey NM, Zaorsky NG, Galloway TJ. The role of radiation therapy in the management of sialorrhea: A systematic review. Laryngoscope. 2016;126(1):80-5.
89. Zeilstra LJ, Vissink A, Konings AW, Coppes RP. Radiation induced cell loss in rat submandibular gland and its relation to gland function. Int J Radiat Biol. 2000;76(3):419-29.
90. Wu J, Wang Y, Liu G, Jia Y, Yang J, Shi J, et al. Characterization of air-liquid interface culture of A549 alveolar epithelial cells. Braz J Med Biol Res. 2017;51(2):e6950.
91. Evans RL, Park K, Turner RJ, Watson GE, Nguyen HV, Dennett MR, et al. Severe impairment of salivation in Na+/K+/2Cl- cotransporter (NKCC1)-deficient mice. J Biol Chem. 2000;275(35):26720-6.
92. Hosoi K. Physiological role of aquaporin 5 in salivary glands. Pflugers Arch. 2016;468(4):519-39.
93. Singh VK, Seed TM. The efficacy and safety of amifostine for the acute radiation syndrome. Expert Opin Drug Saf. 2019;18(11):1077-90.
94. King M, Joseph S, Albert A, Thomas TV, Nittala MR, Woods WC, et al. Use of Amifostine for Cytoprotection during Radiation Therapy: A Review. Oncology. 2020;98(2):61-80.
95. Hwang WYK, Koh LP, Ng HJ, Tan PHC, Chuah CTH, Fook SC, et al. A randomized trial of amifostine as a cytoprotectant for patients receiving myeloablative therapy for allogeneic hematopoietic stem cell transplantation. Bone Marrow Transpl. 2004;34(1):51-6.
96. Kouvaris JR, Kouloulias VE, Vlahos LJ. Amifostine: the first selective-target and broad-spectrum radioprotector. Oncologist. 2007;12(6):738-47.
97. Varghese JJ, Schmale IL, Mickelsen D, Hansen ME, Newlands SD, Benoit DSW, et al. Localized Delivery of Amifostine Enhances Salivary Gland Radioprotection. J Dent Res. 2018;97(11):1252-9.
98. Brizel DM, Wasserman TH, Henke M, Strnad V, Rudat V, Monnier A, et al. Phase III randomized trial of amifostine as a radioprotector in head and neck cancer. J Clin Oncol. 2000;18(19):3339-45.
99. Simone NL, Menard C, Soule BP, Albert PS, Guion P, Smith S, et al. Intrarectal amifostine during external beam radiation therapy for prostate cancer produces significant improvements in Quality of Life measured by EPIC score. Int J Radiat Oncol Biol Phys. 2008;70(1):90-5.
100. Spencer CM, Goa KL. Amifostine. A review of its pharmacodynamic and pharmacokinetic properties, and therapeutic potential as a radioprotector and cytotoxic chemoprotector. Drugs. 1995;50(6):1001-31.
101. Culy CR, Spencer CM. Amifostine: an update on its clinical status as a cytoprotectant in patients with cancer receiving chemotherapy or radiotherapy and its potential therapeutic

application in myelodysplastic syndrome. Drugs. 2001;61(5):641-84.
102. Koukourakis MI, Giatromanolaki A, Zois CE, Kalamida D, Pouliliou S, Karagounis IV, et al. Normal tissue radioprotection by amifostine via Warburg-type effects. Sci Rep. 2016;6:30986.
103. Takahashi I, Nagai T, Miyaishi K, Maehara Y, Niibe H. Clinical study of the radioprotective effects of Amifostine (YM-08310, WR-2721) on chronic radiation injury. Int J Radiat Oncol Biol Phys. 1986;12(6):935-8.
104. Armstrong WR, Gafita A, Zhu S, Thin P, Nguyen K, Alano R, et al. The Impact of Monosodium Glutamate on (68)Ga-PSMA-11 Biodistribution in Men with Prostate Cancer: A Prospective Randomized, Controlled Imaging Study. J Nucl Med. 2021;62(9):1244-51.
105. Rousseau E, Lau J, Kuo HT, Zhang Z, Merkens H, Hundal-Jabal N, et al. Monosodium Glutamate Reduces (68)Ga-PSMA-11 Uptake in Salivary Glands and Kidneys in a Preclinical Prostate Cancer Model. J Nucl Med. 2018;59(12):1865-8.
106. Ramachandran L. Radioprotection by tempol: Studies on tissue antioxidant levels, hematopoietic and gastrointestinal systems, in mice whole body exposed to sub- lethal doses of gamma radiation. Iranian Journal of Radiation Research. 2012;10(1):1-10.
107. Kudo W, Yamato M, Yamada K, Kinoshita Y, Shiba T, Watanabe T, et al. Formation of TEMPOL-hydroxylamine during reaction between TEMPOL and hydroxyl radical: HPLC/ECD study. Free Radic Res. 2008;42(5):505-12.
108. Dittmann KH, Mayer C, Rodemann HP. Radioprotection of normal tissue to improve radiotherapy: the effect of the Bowman Birk protease inhibitor. Curr Med Chem Anticancer Agents. 2003;3(5):360-3.
109. Chandra A, Wang L, Young T, Zhong L, Tseng WJ, Levine MA, et al. Proteasome inhibitor bortezomib is a novel therapeutic agent for focal radiation-induced osteoporosis. FASEB J. 2018;32(1):52-62.
110. Liu Z, Dong L, Zheng Z, Liu S, Gong S, Meng L, et al. Mechanism, Prevention, and Treatment of Radiation-Induced Salivary Gland Injury Related to Oxidative Stress. Antioxidants (Basel). 2021;10(11).
111. Calderwood SK, Gong J. Heat Shock Proteins Promote Cancer: It's a Protection Racket. Trends Biochem Sci. 2016;41(4):311-23.
112. Shevtsov M, Balogi Z, Khachatryan W, Gao H, Vigh L, Multhoff G. Membrane-Associated Heat Shock Proteins in Oncology: From Basic Research to New Theranostic Targets. Cells. 2020;9(5).
113. Kibbey MC, Royce LS, Dym M, Baum BJ, Kleinman HK. Glandular-like morphogenesis of the human submandibular tumor cell line A253 on basement membrane components. Exp Cell Res. 1992;198(2):343-51.
114. Organoid vs Primary Cell 3D Culture Crown Bioscience [Available from: https://blog.crownbio.com/how-are-organoids-different-from-3d-primary-cell-cultures.
115. Kapalczynska M, Kolenda T, Przybyla W, Zajaczkowska M, Teresiak A, Filas V, et al. 2D and 3D cell cultures - a comparison of different types of cancer cell cultures. Arch Med Sci. 2018;14(4):910-9.
116. Tanaka J, Mishima K. In vitro three-dimensional culture systems of salivary glands. Pathol Int. 2020;70(8):493-501.
117. Dolega ME, Abeille F, Picollet-D'hahan N, Gidrol X. Controlled 3D culture in Matrigel microbeads to analyze clonal acinar development. Biomaterials. 2015;52:347-57.
118. Benton G, Arnaoutova I, George J, Kleinman HK, Koblinski J. Matrigel: from discovery and ECM mimicry to assays and models for cancer research. Adv Drug Deliv Rev. 2014;79-80:3-18.

119. Tse HM, Gardner G, Dominguez-Bendala J, Fraker CA. The Importance of Proper Oxygenation in 3D Culture. Front Bioeng Biotechnol. 2021;9:634403.
120. Corning® Matrigel® Matrix for Organoid Culture Corning [Available from: https://www.corning.com/emea/en/products/life-sciences/products/surfaces/matrigel-matrix-for-organoids.html.
121. Corning® Matrigel® Matrix Corning [Available from: https://www.corning.com.
122. Shandilya UK, Sharma A, Sodhi M, Kapila N, Kishore A, Mohanty A, et al. Matrix-based three-dimensional culture of buffalo mammary epithelial cells showed higher induction of genes related to milk protein and fatty acid metabolism. Cell Biol Int. 2016;40(2):232-8.
123. Gargotti M, Lopez-Gonzalez U, Byrne HJ, Casey A. Comparative studies of cellular viability levels on 2D and 3D in vitro culture matrices. Cytotechnology. 2018;70(1):261-73.
124. Zhao C, Meng C, Cui N, Sha J, Sun L, Zhu D. Organoid Models for Salivary Gland Biology and Regenerative Medicine. Stem Cells Int. 2021;2021:9922597.
125. Yoon Y-J, Kim D, Tak KY, Hwang S, Kim J, Sim NS, et al. Salivary gland organoid culture maintains distinct glandular properties of murine and human major salivary glands. Nature Communications. 2022;13(1):3291.
126. Noll BD, Grdzelishvili A, Brennan MT, Mougeot FB, Mougeot JC. Immortalization of Salivary Gland Epithelial Cells of Xerostomic Patients: Establishment and Characterization of Novel Cell Lines. J Clin Med. 2020;9(12).
127. Loureiro CA, Barros P, Matos P, Jordan P. Tyrosine phosphorylation modulates cell surface expression of chloride cotransporters NKCC2 and KCC3 (vol 669, pg 61, 2019). Archives of Biochemistry and Biophysics. 2021;704.
128. Ren H, Birch NP, Suresh V. An Optimised Human Cell Culture Model for Alveolar Epithelial Transport. Plos One. 2016;11(10).
129. Laube M, Bossmann M, Thome UH. Glucocorticoids Distinctively Modulate the CFTR Channel with Possible Implications in Lung Development and Transition into Extrauterine Life. Plos One. 2015;10(4).
130. Nielsen S, Frokiaer J, Marples D, Kwon TH, Agre P, Knepper MA. Aquaporins in the kidney: from molecules to medicine. Physiol Rev. 2002;82(1):205-44.
131. Russell JM. Sodium-potassium-chloride cotransport. Physiol Rev. 2000;80(1):211-76.
132. Nickerson AJ, Rajendran VM. Aldosterone up-regulates basolateral Na(+) -K(+) -2Cl(-) cotransporter-1 to support enhanced large-conductance K(+) channel-mediated K(+) secretion in rat distal colon. FASEB J. 2021;35(5):e21606.
133. Li YC, Tian YQ, Wu YY, Xu YC, Zhang PA, Sha J, et al. Upregulation of Spinal ASIC1 and NKCC1 Expression Contributes to Chronic Visceral Pain in Rats. Front Mol Neurosci. 2020;13:611179.
134. Muroi SI, Isohama Y. Ezrin Regulates Ca(2+) Ionophore-Induced Plasma Membrane Translocation of Aquaporin-5. Int J Mol Sci. 2021;22(24).
135. Zhou B, Stueve TR, Mihalakakos EA, Miao L, Mullen D, Wang Y, et al. Comprehensive epigenomic profiling of human alveolar epithelial differentiation identifies key epigenetic states and transcription factor co-regulatory networks for maintenance of distal lung identity. BMC Genomics. 2021;22(1):906.
136. Mo YQ, Nakamura H, Tanaka T, Odani T, Perez P, Ji Y, et al. Lysosomal exocytosis of HSP70 stimulates monocytic BMP6 expression in Sjogren's syndrome. J Clin Invest. 2022;132(6).

137. Kim J, Lee SW, Park K. CXCR4 Regulates Temporal Differentiation via PRC1 Complex in Organogenesis of Epithelial Glands. Int J Mol Sci. 2021;22(2).
138. Patino-Garcia D, Rocha-Perez N, Moreno RD, Orellana R. Antigen retrieval by citrate solution improves western blot signal. Methodsx. 2019;6:464-8.
139. D'Amico F, Skarmoutsou E, Stivala F. State of the art in antigen retrieval for immunohistochemistry. J Immunol Methods. 2009;341(1-2):1-18.
140. Hoetelmans RW, van Slooten HJ, Keijzer R, van de Velde CJ, van Dierendonck JH. Comparison of the effects of microwave heating and high pressure cooking for antigen retrieval of human and rat Bc1-2 protein in formaldehyde-fixed, paraffin-embedded sections. Biotech Histochem. 2002;77(3):137-44.
141. Kashir J, Buntwal L, Nomikos M, Calver BL, Stamatiadis P, Ashley P, et al. Antigen unmasking enhances visualization efficacy of the oocyte activation factor, phospholipase C zeta, in mammalian sperm. Mol Hum Reprod. 2017;23(1):54-67.
142. Shi SR, Chaiwun B, Young L, Cote RJ, Taylor CR. Antigen retrieval technique utilizing citrate buffer or urea solution for immunohistochemical demonstration of androgen receptor in formalin-fixed paraffin sections. J Histochem Cytochem. 1993;41(11):1599-604.
143. Taylor CR, Shi SR, Chaiwun B, Young L, Imam SA, Cote RJ. Strategies for improving the immunohistochemical staining of various intranuclear prognostic markers in formalin-paraffin sections: androgen receptor, estrogen receptor, progesterone receptor, p53 protein, proliferating cell nuclear antigen, and Ki-67 antigen revealed by antigen retrieval techniques. Hum Pathol. 1994;25(3):263-70.
144. Ghosh R, Gilda JE, Gomes AV. The necessity of and strategies for improving confidence in the accuracy of western blots. Expert Rev Proteomics. 2014;11(5):549-60.
145. Pauwels B, Korst AE, de Pooter CM, Lambrechts HA, Pattyn GG, Lardon F, et al. The radiosensitising effect of gemcitabine and the influence of the rescue agent amifostine in vitro. Eur J Cancer. 2003;39(6):838-46.
146. Ribizzi I, Darnowski JW, Goulette FA, Sertoli MR, Calabresi P. Amifostine cytotoxicity and induction of apoptosis in a human myelodysplastic cell line. Leuk Res. 2000;24(6):519-25.
147. Huang B, He T, Yao Q, Zhang L, Yao Y, Tang H, et al. Amifostine Suppresses the Side Effects of Radiation on BMSCs by Promoting Cell Proliferation and Reducing ROS Production. Stem Cells Int. 2019;2019:8749090.
148. Orellana EA, Kasinski AL. Sulforhodamine B (SRB) Assay in Cell Culture to Investigate Cell Proliferation. Bio Protoc. 2016;6(21).
149. In Vitro Toxicology Assay Kit, Sulforhodamine B based Sigma Aldrich [Available from: https://www.sigmaaldrich.com/BE/en/product/sigma/tox6.
150. Vichai V, Kirtikara K. Sulforhodamine B colorimetric assay for cytotoxicity screening. Nat Protoc. 2006;1(3):1112-6.
151. Zhou H, Weir MD, Xu HH. Effect of cell seeding density on proliferation and osteodifferentiation of umbilical cord stem cells on calcium phosphate cement-fiber scaffold. Tissue Eng Part A. 2011;17(21-22):2603-13.
152. Ng NS, Ooi L. A Simple Microplate Assay for Reactive Oxygen Species Generation and Rapid Cellular Protein Normalization. Bio Protoc. 2021;11(1):e3877.
153. Papazisis KT, Geromichalos GD, Dimitriadis KA, Kortsaris AH. Optimization of the sulforhodamine B colorimetric assay. J Immunol Methods. 1997;208(2):151-8.

154. Pauwels B, Korst AE, de Pooter CM, Pattyn GG, Lambrechts HA, Baay MF, et al. Comparison of the sulforhodamine B assay and the clonogenic assay for in vitro chemoradiation studies. Cancer Chemother Pharmacol. 2003;51(3):221-6.
155. Meyer R, Wong WY, Guzman R, Burd R, Limesand K. Radiation Treatment of Organotypic Cultures from Submandibular and Parotid Salivary Glands Models Key In Vivo Characteristics. J Vis Exp. 2019(147).
156. Limesand KH, Avila JL, Victory K, Chang HH, Shin YJ, Grundmann O, et al. Insulin-like growth factor-1 preserves salivary gland function after fractionated radiation. Int J Radiat Oncol Biol Phys. 2010;78(2):579-86.
157. Victory K, Burd R, Fribley A, Sittadjody S, Arnett D, Klein RR, et al. Head and neck tumor cell radiation response occurs in the presence of IGF1. J Dent Res. 2011;90(3):347-52.
158. Yang X, Ding Y, Ji T, Zhao X, Wang H, Zhao X, et al. Improvement of the in vitro safety profile and cytoprotective efficacy of amifostine against chemotherapy by PEGylation strategy. Biochem Pharmacol. 2016;108:11-21.
159. Taylor CW, Wang LM, List AF, Fernandes D, Paine-Murrieta GD, Johnson CS, et al. Amifostine protects normal tissues from paclitaxel toxicity while cytotoxicity against tumour cells is maintained. Eur J Cancer. 1997;33(10):1693-8.
160. Pereira AF, Lino JA, Alves BWF, Lisboa MRP, Pontes RB, Leite C, et al. Amifostine protects from the peripheral sensory neuropathy induced by oxaliplatin in mice. Braz J Med Biol Res. 2020;53(11):e10263.
161. Andersson C, Zhang AL, Roomans GM. CA(2+) mobilization in the human submandibular duct cell line A253. Cell Biol Int. 2000;24(5):273-7.
162. Tai G, Zhang H, Du J, Chen G, Huang J, Yu J, et al. TIGAR overexpression diminishes radiosensitivity of parotid gland fibroblast cells and inhibits IR-induced cell autophagy. Int J Clin Exp Pathol. 2015;8(5):4823-9.
163. Hs 917.T ATCC [Available from: https://www.atcc.org/products/crl-7669.
164. Paardekooper GM, Cammelli S, Zeilstra LJ, Coppes RP, Konings AW. Radiation-induced apoptosis in relation to acute impairment of rat salivary gland function. Int J Radiat Biol. 1998;73(6):641-8.
165. van Leeuwen CM, Oei AL, Crezee J, Bel A, Franken NAP, Stalpers LJA, et al. The alfa and beta of tumours: a review of parameters of the linear-quadratic model, derived from clinical radiotherapy studies. Radiat Oncol. 2018;13(1):96.
166. Lo HC, Hsu JH, Lai LC, Tsai MH, Chuang EY. MicroRNA-107 enhances radiosensitivity by suppressing granulin in PC-3 prostate cancer cells. Sci Rep. 2020;10(1):14584.
167. M.Yashar C. Clinical Gynecologic Oncology. 9 ed2018.
168. Hawkins RB. Effect of heterogeneous radio sensitivity on the survival, alpha beta ratio and biologic effective dose calculation of irradiated mammalian cell populations. Clin Transl Radiat Oncol. 2017;4:32-8.
169. Gupta K, Vuckovic I, Zhang S, Xiong Y, Carlson BL, Jacobs J, et al. Radiation Induced Metabolic Alterations Associate With Tumor Aggressiveness and Poor Outcome in Glioblastoma. Front Oncol. 2020;10:535.
170. Tang L, Wei F, Wu Y, He Y, Shi L, Xiong F, et al. Role of metabolism in cancer cell radioresistance and radiosensitization methods. J Exp Clin Cancer Res. 2018;37(1):87.
171. LIVE/DEAD Cell Viability Assays ThermoFisher [Available from: https://www.thermofisher.com/.

Acknowledgements - I am thankful to Heynickx Nathalie and Vermeulen Koen for the supervision and feedback, to Segers Charlotte for the help, everyone of the department of radiobiology at SCK CEN for the help and to my family for the love and support. Figure 1, 2 and 4 were created in Biorender.

Author contributions - Heynickx Nathalie and Vermeulen Koen conceived and designed the research. Breugelmans Rosanne, Heynickx Nathalie, Vermeulen Koen and Segers Charlotte performed experiments and data analysis. Breugelmans Rosanne wrote the paper. All authors carefully edited the manuscript.

SUPPLEMENTARY FIGURES

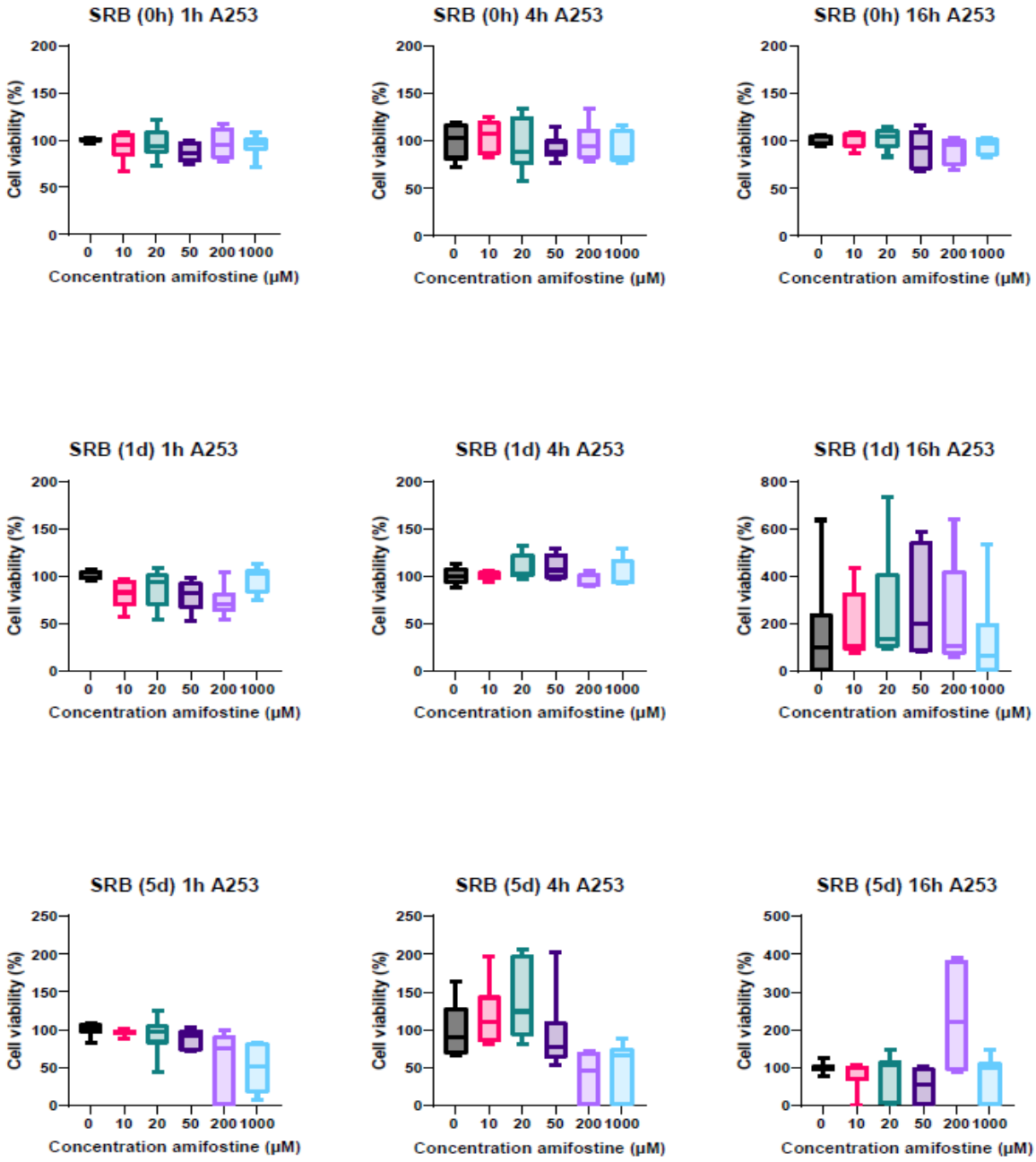

Figure S1: Cytotoxicity of amifostine in A-253 cells. Cytotoxicity after incubation with amifostine for 1, 4 or 16 hours. Cells were fixated after 0, 1 or 5 days with different concentrations of amifostine. All results are normalized to the untreated cells.. N=6

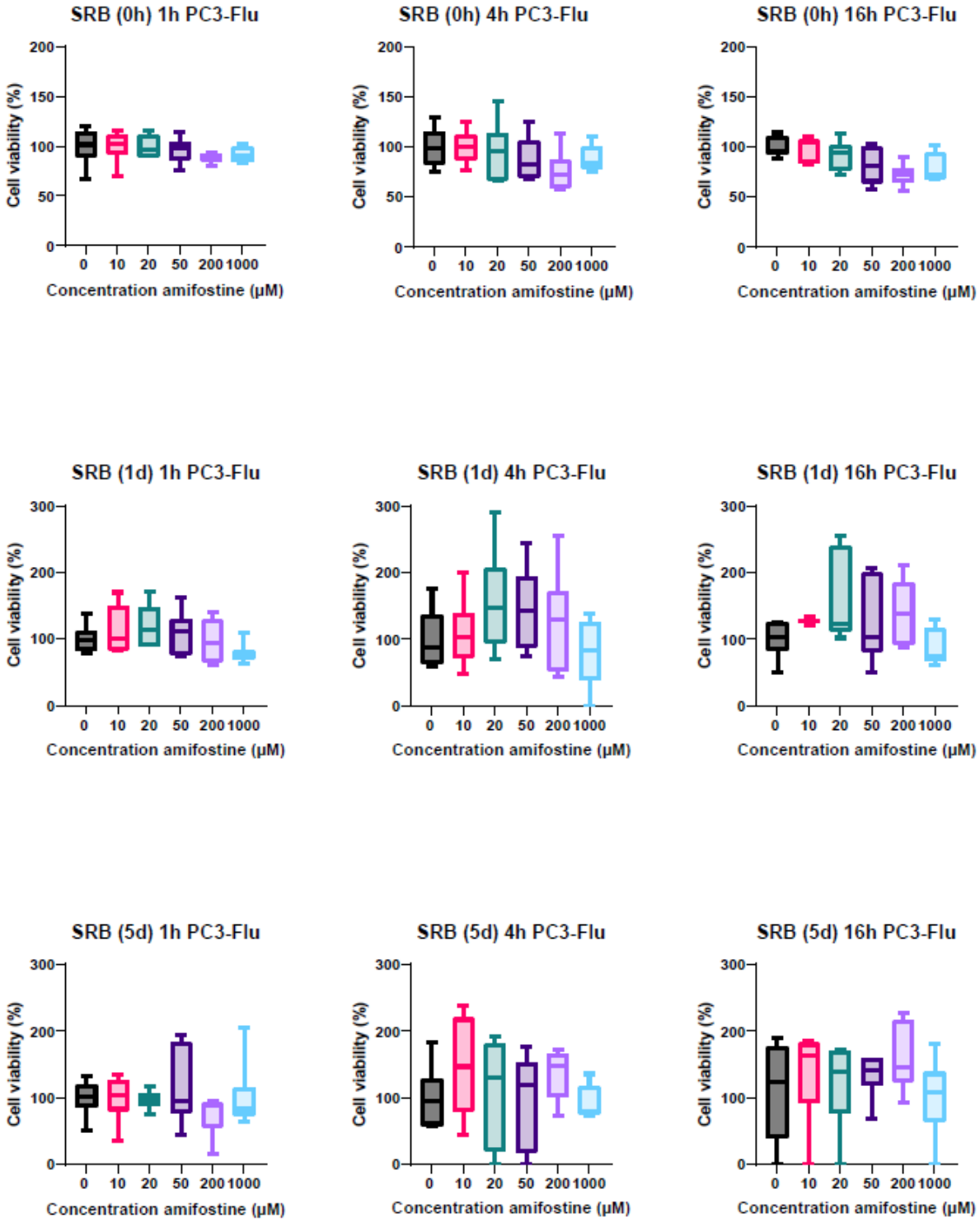

Figure S2: Cytotoxicity of amifostine in PC3-Flu cells. Cytotoxicity after incubation with amifostine for 1, 4 or 16 hours. Cells were fixated after 0, 1 or 5 days with different concentrations of amifostine. All results are normalized to the untreated cells.. N=6

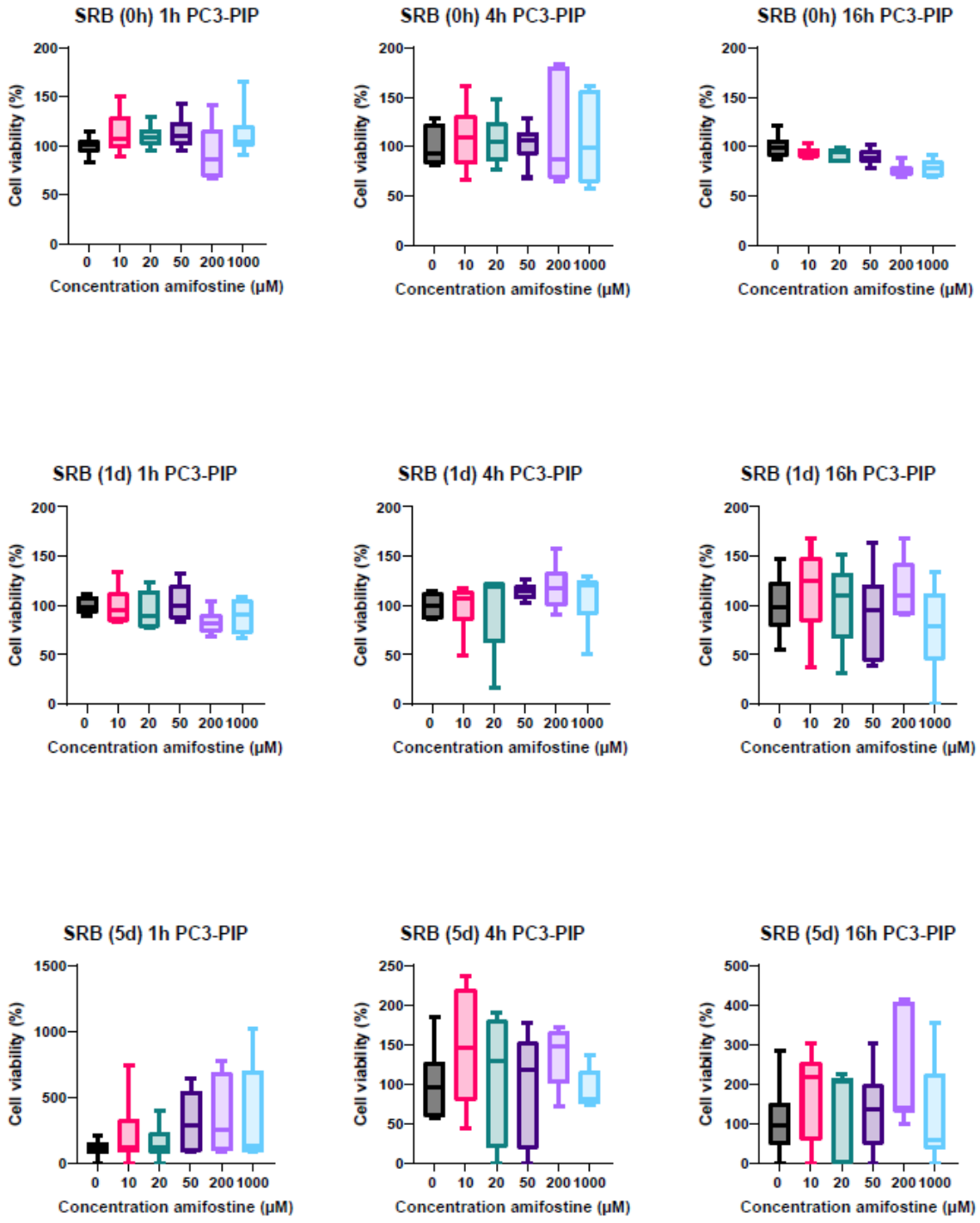

Figure S3: Cytotoxicity of amifostine in PC3-PIP cells. Cytotoxicity after incubation with amifostine for 1, 4 or 16 hours. Cells were fixated after 0, 1 or 5 days with different concentrations of amifostine. All results are normalized to the untreated cells.. N=6